A Study on Deducing Imapct of Loss of Vegetation Cover changes on Land Surface Temperature

THESIS
SUBMITTED IN PARTIAL FULFILMENT OF THE
REQUIREMENTS FOR THE DEGREE OF

Master of Technology

in

Agricultural Engineering

(Soil and Water Conservation Engineering)

Submitted by

Gopal Kumar

Supervisor

Dr. V.K. Chandola

Co-Supervisor

Dr. P.K. Srivastava

DEPARTMENT OF FARM ENGINEERING
INSTITUTE OF AGRICULTURAL SCIENCES
BANARAS HINDU UNIVERSITY
VARANASI – 221 005
INDIA

ID. No. 19412AEN007 2022 Enrolment No. 416309

काशी हिन्दू विश्वविद्यालय BANARAS HINDU UNIVERSITY

Ref. No. …… **Date ……**

CERTIFICATE

To,
The Registrar (Academic)
Banaras Hindu University
Varanasi–221005
U.P., India

Through: The Head, Department of Farm Engineering, I. Ag. Sc., BHU, Varanasi.

Dear Sir,

We have great pleasure in forwarding the thesis entitled **"A Study on Deducing Impact of Loss of Vegetation Cover Changes on Land Surface Temperature"** submitted by **Mr. Gopal Kumar**, **ID. No. 19412AEN007**, **Enrolment No. 416309** in partial fulfillment of the requirements for the award of the degree of **Master of Technology** in **Agricultural Engineering (Soil and Water Conservation Engineering)**, Department of Farm Engineering, Institute of Agricultural Sciences, Banaras Hindu University, Varanasi.

This is to certify that the work has been carried out solely by Mr. Gopal Kumar under our supervision and findings of her thesis presented herein are genuine and original to the best of our knowledge and no part of the work has been submitted for any other degree or distinction.

Thanking you, Yours faithfully

FORWARDED BY

Dr. V.K. Chandola (Supervisor)
Professor
Department of Farm Engineering
Institute of Agricultural Sciences
Banaras Hindu University, Varanasi, U.P.

HEAD

Dr. Prashant Kumar Srivastava (Co-supervisor)
Assistant Professor
Institute of Environment & Sustainable Development
BHU

A Study on Deducing Impact of Loss of Vegetation Cover Changes on Land Surface Temperature

By

Gopal Kumar

Thesis submitted in the partial fulfilment of
the requirements for the degree of

Master of Technology
in
Agricultural Engineering
(Soil and Water Conservation Engineering)

DEPARTMENT OF FARM ENGINEERING
INSTITUTE OF AGRICULTURAL SCIENCES
BANARAS HINDU UNIVERSITY
VARANASI – 221 005

ID. No. 19412AEN007 **2022** **Enrolment No. 416309**

THESIS APPROVED BY ADVISORY COMMITTEE

Chairman
Dr. V.K. Chandola
Professor
Department of Farm Engineering
Institute of Agricultural Sciences
Banaras Hindu University, Varanasi, U.P.

Co-Supervisor
Dr. Prashant Kumar Srivastava
Assistant Professor
Institute of Environment and Sustainable Development
Banaras Hindu University, Varanasi, U.P

Member
Dr. A.K. Nema
Professor and Head
Department of Farm Engineering
Institute of Agricultural Sciences
Banaras Hindu University, Varanasi, U.P.

Member
Dr. Ramesh Kumar Singh
Professor
Department of Agronomy
Institute of Agricultural Sciences
Banaras Hindu University, Varanasi, U.P.

External Examiner

CERTIFICATE

We, the undersigned members of the advisory committee of Mr. Gopal Kumar, ID. No. 19412AEN007, a candidate for the degree of **Master of Technology** in **Agricultural Engineering (Soil and Water Conservation Engineering)**, agree that the thesis entitled **"A Study on Deducing Impact of Loss of Vegetation Cover Changes on Land Surface Temperature. "** may be submitted in partial fulfillment of the requirements for the degree.

Chairman
Dr. V.K. Chandola
Professor
Department of Farm Engineering
Institute of Agricultural Sciences
Banaras Hindu University, Varanasi, U.P.

Co-Supervisor
Dr. Prashant Kumar Srivastava
Assistant Professor
Institute of Environment and Sustainable Development
Banaras Hindu University, Varanasi, U.P

Member
Dr. A.K. Nema
Professor
Department of Farm Engineering
Institute of Agricultural Sciences
Banaras Hindu University, Varanasi, U.P.

Member
Dr. Ramesh Kumar Singh
Professor
Department of Agronomy
Institute of Agricultural Sciences
Banaras Hindu University, Varanasi, U.P.

External Examiner

ACKNOWLEDGEMENT

While I stand at the edge of completion of my research work, my mind is flooded with numerous memories of the last two years which are full of showing gratefulness to those who have consistently and continuously helped me at various stages of my research work. I am grateful to almighty that he enriched my life with such superb, kind and nice people and this is a wonderful occasion to say thanks, express my gratitude, respect, and love to the people, who enchanted and mesmerized me with their talent, skill, knowledge and care in every step of my life.

Firstly, I am grateful to the noted educationist, freedom fighter and the founder of prestigious Banaras Hindu University, ***Bharat Ratna, Mahamana Pt. Madan Mohan Malviya Ji****, under whom shadow I completed my research work.*

Then, I wish to express my special thanks to my honorable advisor, ***Dr. V.K.Chandola****, Professor, Department of Farm Engineering, Institute of Agricultural Sciences, Banaras Hindu University, Varanasi, for his perfect advice, proper guidelines, constant encouragement and co-operation. His persistent help and monitoring helped me in the culmination of my research, from the thesis proposal up to the thesis manuscript.*

I am highly obliged to ***Dr. Prashant Kumar Srivastava,*** *Assistant Professor, Institute of Environment and Sustainable Development, Banaras Hindu University, Varanasi, U.P., for his invaluable guidance, valuable suggestions and encouragement throughout research work.*

I avail this opportunity to express my deep sense of gratitude and indebtedness to ***Prof. Yashwant Singh,*** *Dean and Director, Institute of Agricultural Sciences, Banaras Hindu University, for their valuable suggestion, inspiring and constructive criticism and parental affection throughout the present investigation up to the finalization of the manuscripts of the thesis.*

I will remain grateful to all the non-teaching staff members, especially ***Mr. O.P. Singh*** *and* ***Mr. Uma*** *of the Department of Farm Engineering for their co-operation throughout the course of my study.*

I would also like to extend special thanks to ***Ms. Prachi Singh****, Research Scholar, IESD without her assistance and dedicated involvement in every step throughout the process, this project would have never been accomplished. I would like to thank her very much for her support and understanding.*

I am highly obliged and pay my deep regards to ***Dr. Dileep Kumar Gupta*** *and other laboratory members. I am grateful to Institute of Environment and Sustainable Development, Banaras Hindu University, Varanasi for giving me this opportunity, guidance, encouragement and valuable suggestion during winter internship.*

My heartfelt and special thanks to my seniors, ***Mr. Saswat Kumar Kar, Mr. Dinesh Kumar, Mr. Bhaskar Pratap Singh, Mr. Raj Bahadur, Mr. Kanhu Charan Panda*** *for their kind guidance and co-operation.*

It is a pleasure for me to offer thanks to my M. Tech friends, ***Mr. Ashish Kumar Patel, Mr. Abhishek Singh, Mr. Sujeet Kumar, Ms. Snehil Dubey, Ms. Bhavna Singh, Mr. Krishna Kumar Singh, Mr. Romit Kumar, Mr. Utkarsh Tandon, Mr. Shashi Sekhar Pathak.***

Last but not the least, I record my sincere thanks to my beloved parents and siblings for their encouragement and blessings during my ups and downs. We owe much to all who have directly and indirectly contributed to the success of this research project work.

Date
Place: *(Gopal Kumar)*

CONTENT

LIST OF TABLES

LIST OF FIGURES

CHAPTER 1

INTRODUCTION

Temperature is majority cause for the rapidly changes on the Earth's surface, the importance of Temperature of the land surface (LST) is being increasingly recognised. This will cause glaciers and ice areas to melt, affecting the vegetation in the area. It will have a greater impact in monsoon areas since rainfall is uncertain, and if the monsoon fails, there would be a tremendous downpour of rain. Satellite images are thought to be a useful tool for determining surface temperatures. The use of thermal bands in several of these satellites, including Landsat, makes LST calculation easier.

LSTs is vital for a number of earth science concerns, including urban climatology, global environmental alteration and human environment interaction. Numerous types of land use have been proven to have an influence on the LST and could be used as markers of LST trends. On regional and global dimensions, LST is a crucial parameter in the physics of land-surface processes, incorporating the outcomes of all interactions and energy fluxes between the atmosphere and the ground. LST is influenced by the surface energy balance, the condition of the atmosphere, as well as the surface and subsurface thermal characteristics, and is a main parameter in many environmental models.

The partitioning of heat fluxes, and hence the surface energy response, is a consequence of variable surface soil water-content and vegetation cover, according to LST research. LST readings in non-vegetated locations are typically the radiometric temperatures of bare soil which come under the category of non vegetation. The radiative temperature noted by a sensor approaches, the temperatures of green leaves as the quantity of vegetation cover. The region-based spatio-temporal distribution of LSTs using remote sensing imagery can be utilized as a parameter to support sustainable management with water resource management and landscape planning, as well as in-depth agriculture and agro-environmental studies, in the absence of a condensed network of land-based climatological stations. After adequate aggregation

and parameterisation, one among the most popular significant the applications of the LST derived from satellite data is to evaluate and enhance the worldwide meteorological model forecast. Aside from being required for LST retrieval, surface emissivity can be utilised to distinguish senescent plants. In LULC analysis, LST obtained from remote sensing imagery ia widely used. LST can also be used to track droughts and estimate surface soil moisture, as well as to assess wheat water requirements and predict frosts in orange groves.

However, due to the limitation of the ground measurements of LTS over a range of spatial and time scales are extremely difficult to achieve. Meteorological stations and ground surveys are frequently sporadically or unevenly dispersed in difficult terrain, such as the Himalayas, and they also tend to be prejudiced because they often favour dense forests and hilly terrains. Adanced geospatial interpolation approaches remain difficult to apply in complex terrains. Remote sensing data, on the other hand, has become more widely available, allowing for the analysis of the spatial distribution of energy balance components such as surface temperature and albedo. Traditional geospatial interpolation methods remain difficult to apply in complex terrains. Remote sensing data, on the other hand, has become more widely available, allowing for the analysis of the the geographical distribution of energy balance components such as surface temperature and albedo. Many land surface models are based on remote sensing techniques include LST as a important boundary condition (Wan *et al.* 2002). Satellite thermal sensing has recently improved in accuracy due to higher resolution, thanks to advancements in remote sensing technologies and multi-sensor datasets, and new image processing techniques, allowing LST evaluation. Landsat Enhanced Thematic Mapper Plus (Landsat ETM+), Advanced Spaceborne - Thermal Emission and Reflection Radiometer (ASTER), Advanced Very High Resolution - Radiometer (AVHRR), and Geostationary Orbiting Environmental Satellite (GOES) advanced multispectral satellites have all been used to estimate LST. According to the result of present study they have found that Remote sensing using thermal infrared (TIR) technology is the sole way to recover LSTs over broad areas of the Earth's surface at various spatial resolutions and periodicities. To extract LST values from satellite TIR data, several factors must be quantified, including sensor

radiometric calibrations, atmospheric correction, surface emissivity correction, spatial inconsistency over land cover characterisation, and the combined effects of viewing geometry, background, and fractional vegetative cover.

Land surface remote sensing data have been used to create models of land surface-atmosphere interaction and to investigate the link between temperature and LULC. Some research used fundamental surface descriptors like vegetation fraction instead of qualitative LULC classifications to evaluate the effect of biophysical factors on LST. The vegetation index-LST relationship has been utilised to extract sub-pixel thermal changes and analyse land cover trends, as well as to obtain surface biophysical data. A negative link between vegetation and LST has been noticed by many researchers. This discovery sparked more investigation into two key paths: statistical examination of the link and the temperature/vegetation index (TVX) approach. By definition, TVX is a multi-spectral approach for observing the relationships between LST and a vegetation index (VI) on a scatterplot.

1.1 Global forest status

Globally forest cover leads to 31 percent of the world's land surface area and contains a large amount of terrestrial biodiversity. Whereas approximately half of the forest is comparatively intact and primary forest (i.e., naturally regenerated and significantly distribution of native species with no involvement of human activities) are cover more than $1/3^{rd}$ of the area (Taubert *et al.*, 2018). The total area of forest cover is about 4.06 billion hectares or approximately (50*100 m) i.e., $5000m^2$ per person (Mayaux *et al.*, 1998), but the forest is not equally distributed geographically. The world's largest proportion of forest is tropical i.e., 45 percent followed by temperate, boreal, and subtropical forest types. Forest biodiversity is an appearance of the differences of living organisms that are present in the ecosystem and it is considered as one of the estimations mean of forest health and its stability. Forests contribute extensively to the conservation of terrestrial biodiversity (Newbold *et al.*, 2014).

The tropical forest is distributed in tropical regions i.e., forest area approximately bounded and followed by Tropic of Cancer and Capricorn (23° N and 23° S) (Putz and Redford, 2010). The tropical zone is predominantly affected by wind circulation patterns recognized as the Hadley cell. Forest in temperate areas are willingly categorized on basis of tree canopy but in contrast, it is difficult to categorize in the case of tropical forest (Lobovikov *et al*., 2007). Around 80 percent of the globally documented species are found in tropical rainforests even they cover only 6 percent of the earth's land surface (D'Annunzio *et al*., 2014). The tropical forest is often supposed to be a moist forest with annual rainfall over 4000 mm and an Evergreen rainforest with no month receiving less than 100 mm of precipitation. But forests in this zone are mainly based on elevation, soil type, and forest structure due to geographical distribution (Mackey *et al*., 2020). The remaining major forests are Tropical dry forest (known as monsoon forest) and Semi-evergreen rain forest. Other than these there are Lowland evergreen rainforest, Semi-evergreen rainforest, Dry-deciduous forest, Lower montane forest, Upper montane forest, Health forest, Mangroves, Freshwater swamp forest, and peat swamp forest (Davies *et al*., 2021). Tropical forests are recognized as global epicenters and superficial modulators governing climate change by their structural organization, adaptivity to dry climate, spatial heterogeneity irregular precipitation and moisture stress.

According to India State Forest Report (ISFR), 2017 total forest area and tree cover are about 29 202,088 sq. km which is 24.38 percent of the total geographical area of India (Ao *et al*., 2021). Forest is the major environmental resource and it grew at 0.7 percent annually throughout 2000-2010. In India, forests are mainly Tropical Wet Forest, Tropical Moist Forest, Tropical Dry Deciduous forest, Sub-Tropical Dry Evergreen Forest, Himalayan Moist Temperate Forest, Sub Alpine, Alpine Scrub Forest, and so on.

1.2 Remote sensing data used in the assessment

Recently remotely sensed data have provided help to predict, estimate and map forests at various levels. Satellite remote sensing (SRS) is proven as an extremely powerful tool because it allows for spatial coverage of a larger region in a short period. and provide a continuous source of ground data information globally (He *et*

al., 2015). It can play a key role in establishing a baseline for monitoring and analysis as well as cost-effectiveness as compared to traditional inventories and assessments. Nowadays satellite remote sensing data represents a powerful tool for researchers to acknowledge the spatial-temporal distribution of biodiversity in the period of major environmental change worldwide (Pettorelli *et al.*, 2014). As space-borne remote sensing collects large land-covered geographically distributed areas on regular intervals and its different levels of spatial details. Satellite remote sensing is one of the most leading and cost-effective methods to identify biodiversity and compute changes in species composition.

Many drawbacks are associated with the use of remotely sensed data for predicting biophysical parameters, as deriving there measures from the spatial and spectral signature of an environmental structure are not trivial. In contrast, the encroachments of remote sensors, data characteristics, and processing systems have enhanced satellite imagery potential to provide accurate and vigorous spatially precise estimates of LST (Gyamfi-Ampadu *et al.*, 2021). Satellite remote sensing has been playing a crucial role in forest monitoring, management assessment, and conservation. The productivity of these estimations has demonstrated remote sensing satellite imagery ability for the prediction of the biophysical parameters based on field obtained measured data. Besides, many of these studies propose images and approaches that could be approved in the modeling process.

1.3 Objectives

1) Multi-spectral data processing for estimation top of atmosphere reflectance from LANDSAT images
2) To calculate LST for the Pindari area of Garhwal Division from LANDSAT imagery for a multi-decadal analysis from 2000 to 2020
3) LULC classification to analyse the resulting temporal and spatial variations.
4) Study the change in vegetation cover during the year 2000 to 2020.

CHAPTER 2

LITERATURE REVIEW

Rajan *et al.* (2013) had studied on central Western Ghats and temporal land cover analysis is done through NDVI reveals the transition of vegetation from 96.13 (1989) to 89.07% (2009). Land use land cover analysis was done using supervised classifier which purely based on Gaussian maximum likelihood classifier reveals the decline of forests from 57.65% (1989) to 39.78% (2009). Presented study based on the altering land use to the altering land surface temperature at a temporal scale. Various types of thermal signatures of different land use/land cover types also used in the presented study area which helped to provide on their roles in contributing to heat phenomenon. Different Agro-climatic zone wise analysis demonstrate that the amount of vegetation in land use land cover, which has substantial role in moderating the temperatures of a region. It is analysed that coastal and plain regions with smaller spatial amount of vegetation have higher temperatures than other regions of Western Ghats. The results indicate that there is an upsurge of surface temperature from 32.74°C to 41°C. The results suggested that suitable land use preparation to alleviate the enhancement in temperatures by carefully crafting policies for managing anthropogenic forcing of the climate system.

Another study was done by (Imran, Hossain *et al.* 2021) using Remote Sensing data for the several years during summer season in proposed city which, were used to prepare land cover maps, analyze LST to generate various types of hazard maps and further relate the land cover change with LST by using the GIS techniques. According to the findings of this study, the built-up area in the study area rose by 67 percent between 1993 and 2020, mostly by replacing lowland, followed by vegetation, bare soil, and water bodies. The study indicated that the LST ranged from 23.26 to 39.94 °C, 23.69 to 43.35 °C, and 24.44 to 44.58 °C for every 14 years between 1993 and 2020. LST increased by around 0.24 °C per year and human thermal distress shifted from reasonable to robust heat stress for the total study period due to the enhancement of built-up and bare lands. LST was shown to be negatively

connected with the NDVI and the other indices NDWI but favourably correlated with the NDBI, NDBAI.

According to the study of (Falahatkar, Hosseini *et al*. 2011) LST is a crucial metric in urban thermal environment and dynamics research. They suggested a research in Isfahan to assess land cover change detection and the impact of these changes on surface temperature using the TM and ETM+ thermal bands between 1990 and 2001. Land cover maps were constructed using one of the most useful Hybrid method classifications, and changes were discovered using a post-classification comparison study. LST was calculated using a single channel technique. The land cover change map for the years 1990 and 2001 was overlaid with the LST map to investigate the association between land cover categories and land surface temperature. The data show that the maximum surface radiant temperature is found on bare ground (44.9°C in 1990 and 48.9°C in 2001), followed by stony bodies (42.6°C in 1990 and 45.3°C in 2001). Urban and built-up areas have far lower temperatures than barren ground and stony bodies. The Green cover had the lowest radiative temperature between 1990 and 2001 and river classes.

Rapidly urban growth and related land-use land-cover (LULC) change in India have arisen as a serious environmental threat that accelerates the impacts of urban heat island intensity (UHII). (Saha, Bandopadhyay *et al*. 2020) conducted a study using a series of Landsat data. The study primarily focuses on using an integrated model to estimate the near-future LULC scenario and to comprehend the relationship between band mean for specific LULC classes and LST, as well as to generate the temporal association between different types of built-up clusters and LST. The results show that between 1988 and 2018, LST increased from 27.01 to 33.86C, whereas built-up areas increased from 6.93 percent to 27.10 percent. This study detected that the near-future LULC scenario of KMA shows a huge growth of built-up areas paid by reduced vegetation and open spaces. A satisfied correlation (R^2 = 0.84) has been found between band mean and LST in all three Landsat sensors for Landsat 5 TM, for Landsat 7 ETM+ and Landsat 8 OLI correlation were found R^2 = 0.91 and R^2 = 0.88

respectively. However, no satisfied agreement has been found between different built-up clusters and LST over the last 30 years of observation.

Ziaul *et al*. (2017) had studied using multi spectral and temporal satellite data, a study article was published on the influence of LULC on LST in Malda District. In the years 1991, 2010, and 2014, one of the three phases was seasonal and temporal LST analysis. Results indicated that LST increases 0.070°C per year during winter periods and for summer period increases and 0.114°C per year respectively and also presented a significant LST difference occurs over different LULC units. According to the result of LULC Built up area holds maximum LST in all selected three phases. Corelation ranges between NDBI and LST is 0.47 to 0.607 and ranges between NDVI vs. LST from 0.441 to 0.62. LST showed almost co linear relationship with aerial temperature and also gives significant correlation value 0.44604 for January and 0.658 for the month of April 2014. The significance level of 0.01 the temperature gap between ranges varies from 3.5°C to 6.5°C. As a result, the LULC pattern is fast changing, and its imprint is reflected in the LST and air temperature. As a result of the study's findings, immediate thought on new urbanism should be embraced, developed, and implemented in order to stop rising temperatures and the consequences of urban heat islands.

Climate change more effects to Mountainous regions and also more susceptible to recent growths in temperature values. Cameron Highlands has been hampered by increasing land surface temperature (LST) variance due to rising urbanisation and issues of land use/land cover (LULC) difficulties. Study of (How Jin Aik, Ismail *et al*. 2020) explores the influence of the LULC change on LST in the Cameron Highlands during the year ranges from 2009 to 2019 using various types of remote sensing images such as Landsat 7 ETM+, Landsat 8 Operational Land Imager (OLI/TIRS), and Moderate Resolution Imaging Spectroradiometer (MODIS) 11A Thermal sensors. A most successful split-window algorithm was applied to Landsat 8 images during the year 2013–2019 for the retrieval of LST. According to the validation results of the proposed study, the accuracy of was found LULC and LST were more than 94.6% and 80.0%, respectively. It is clearly visible from results the

current trend of urban growth remains at a rate of 0.16% per year, and the area experienced an LST increase of 2°C between 2009 and 2019. To understand the impacts of LULC change, this study is vital for land planners and environmentalists on LST and also useful to propose appropriate policy measures to control development in Cameron Highlands.

Another research was conducted by (Omran 2012) on Ismailia Governorate, Egypt for the investigation of the application of RS/GIS for detecting LULCC and assessing its influence on surface temperature using the Landsat image. Changes was quantifying from 1984 to 2011 year. Firstly, pre-processing of images were done using calibration techniques and geometric and atmospheric corrections were also performed. To find the best band combination Different types of ratios, indices, and optimized index factor were implemented. Most useful Supervised classification such as Maximum Likelihood and spatial reclassification techniques were used.. Six types of land-use/land-cover classes were identified such as urban, vegetation, waterlogged 1 and 2, bare land, and water. According to the result of accuracy assessment highest overall accuracy and Kappa coefficient were found 93.04% and 80.65%, respectively. The combination of RS and GIS technologies was further applied to observe the influence of land-use change on surface temperatures. The Built-up area has swiftly augmented in Ismailia during the 27 years period. The built-up area holds the temperature approx. 37.65°C in 1984 and 43.876°C in 2011) and by Barren land 37.34°C in 1984 and 42.80°C in 2011 which, show the highest surface radiant temperature, vegetated surfaces hold 28.73°C in 1984 and 32.96°C in 2011, and the other class water holds 25.94°C in 1984 and 27.32°C in 2011, waterlogged1 holds 34.54°C in 1984 and 35.60°C in 2011 which, recorded low radiant temperature respectively. Waterlogged2 is the class that shows an unforeseen radiant temperature 26.38°C in 1984 and 27.75°C in 2011. According to the LULC classification urban development was found between 1984 and 2011 has given increase to an average of 6.23°C in surface radiant temperature. During 27 years, the change rate of land-use types which are decreased are barren land 1.12% annually and by waterlogged1 and 2, 0.76 and 6.61% annually. The coverage area by classes is 0.98%, 0.82%, and 0.61% per year by vegetation, water, and built-up, respectively.

On the application of LULC change detection a most successful study was published at Rize, North-East Turkey (Reis 2008). Several types of supervised classification technique were applied to Landsat images during the year of 1976 and 2000. Image Classification of six reflective bands of two Landsat images is carried out by using maximum likelihood method with the use of ground truth data which, obtained from aerial images during the year of 1973 and 2002. The land use land cover changes detection was done using change detection comparison (pixel by pixel). According to the topographic structure the land cover changes are analysed (slope and altitude) by using various types of GIS functions. According to the results unembellished land cover changes have occurred in agricultural (36.2%), urban (117%), pasture (-72.8%) and forestry (-12.8%) areas has been experienced in the region between 1976 and 2000. It was clearly observed that LULC changes were mostly happened in coastal areas and in areas also having low-slung slope values.

CHAPTER 3

MATERIALS AND METHODS

3.1 Study Area

The study area is located in Garhwal which is one of the two administrative divisions of the Indian state of Uttarakhand. Lying in the Himalayas, it is bounded on the north by Tibet, on the east by Kumaon region, on the south by Uttar Pradesh state, and on the northwest by Himachal Pradesh state. Garhwal Himalaya (part of western Himalaya) is spread in seven districts of Uttarakhand and covers an area of 33,412 km^2 . The elevation ranges from 195 metres to 7,816 metres above sea level. Forest types present in the research region include dry deciduous forest, moist deciduous woodland, sal forest, pine forest, temperate and sub-alpine broadleaf forest, alpine scrub, and alpine meadows due to vast topographic differences (Roy *et al*., 2002).

The region plays a essential part in attracting tourists due to its majestic glaciers, wildlife, vegetation richness, cultural richness, scenic beauty and pollution free zone. Char dham badrinath, kedarnath Gangotri , Yamunotri were the lifelong ambition of every religious hindu. This region, with the deficient mineral resources, fragile ecosystem, difficult accessibility welcomes domestic and foreign tourist for economic gains. Whole hill area of Garhwal region is pleasant throughout the summer season that offers the opportunity the tourists to visit the various sites of the region. There are various sites which attract the tourist's community because of its fascinating natural beauty develops due to current weather conditions. Due to erratic patterns of rainfall during the monsoon season from July to August creates this whole region susceptible to various natural disasters, i.e., cloudburst, landslides, and avalanche in upper areas that distracts and discourage the tourist from visiting the region.

3.2 Geological and Geomorphological Diversity of the Region

The area shows a highly dissected antecedent drainage system. Most of the rivers are originates from glaciers. Various tributaries rivers such as Tons, Aglar, Dhauli, Vishnuganga, Patal Ganga, Mandakini, Pindar, Mandakini and Ramganga are separate catchment on the eastern margin of this region while Yamuna ang ganga are

the main rivers for this area.. Alaknanda and Bhagirathi have their confluence at Deoprayag. After that known as "Holi Ganga," the river movements through Hardwar, Prayagraj, and Varanasi downhearted to the Bay of Bengal. To develop many landforms features glacial and fluvial morphogenic processes are used. The glacial morphogenic procedures have run to the creation of the glacially imprinted landscape in the form of U-shaped valleys. To provide land to the locals for agriculture as well as their settlement glacio-fluvial deposits have been already assumed increase to a number of terraces which are fairly extensive. Ultimately, rivers develop a fertile plain land from a long run for agriculture and other economic activities before draining into the Bay of Bangal. The whole alluvial plain is classified into sub-region according to its physiographic characteristics, e.g., younger flood deposits which know as Trai and Nnewer alluvial deposits and Older alluvial deposits are Bhanvar and Bangar.

To control the river course Garhwal Himalaya thrives in a great number of thrusts and faults which have not only restricted the geological identities. Further, these thrusts and faults also distinct Trans, Greater, Lesser, and Shiwalik Himalayan regions next from north to south. Greater Himalaya from Trans, or Tethys Himalayan are separated from Mandhani thrust region which located in the uppermost part of the region. MCT (Main Central Thrust) is closely parallel of the Himalayan terrain and symbols the boundary of smaller Himalaya to the south-central crystalline. Heim and Ganseer (1939) named this thrust in Kali Valley, although Valdiya afterwards advocated and named it Munsiari Thrust.

3.3 Climatic variability of the region

Garhwal Himalaya region is situated in Indian Himalayan monsoonal subcontinent with three main climatic seasons in a year summer (March to June), humid warm (July to June), winter (November to February). This region is observed to be fronting dangerous actions situations due to the erratic design of precipitation during the monsoon season that make this complete hilly region vulnerable to natural disasters such as cloudbursts, landslides, avalanches and flood in plain areas of the region. Decreasion in temperature with the elevation increases is the mutual phenomenon that touches climate spatially and temporal scale at huge. The climatic conditions of the Garhwal Himalayan region differ from the tropical to glacial cover

zone. On the basis of altitude seven different climatic zones were distinguished in the region from south to north i.e. tropical, subtropical, warm, cool temperate, cold, sub-alpine ranges from 3201-4000, and glacial cover more than 4000 m. The climatic variable, temperature and precipitation differ from altitude to altitude. The maximum is found > 39.9°C, 36.1°C, 30.1°C, 24.1°C, 18.1°C, 9.1°C and < 5°C and minimum temperature varies from 6.1°C, 3.1°C, 0.1°C, -2.9°C, -8.9°C and -11.6°C in tropical, sub-tropical, warm temperate, cool temperate, cold temperate, subalpine and glacial cover zones respectively. Various studies were carried out to find the climatic variations and to enquire cause and effects of climate on biotic and abiotic resources. It is suitable and additional practical to improper the climatic regionalization on the improper of elevation (Kaushik, S. D.,1962)

3.4 Soil diversity of the region

Garhwal region is the part of Uttarakhand Himalaya which occupies 32486 Km^2 (60.67%) area and represented highly rugged and fragile topography. The region is dominated by the various landscape features e.g. fauvial V and U-shaped valleys, precipitous ridges, piedmont plain. The highest upper region of the Garhwal covered by glaciers. With the view of geology, physiographically, biologically, climatologically and pedologically, the whole Garhwal region has very diverse and wealthy. Accessibility not only tough due to rugged topography but also rich and dense forest landscapes which provide habitat to its biological diversity. Pine is controlling forest species covers a maximum area of the shiwalik and the lesser Himalayan region. Besides moist temperate, dry deciduous scrub, Sal mixed moist deciduous, Sal, Grassland, Oak, Temperate, coniferous, degraded forest, Dry deciduous, Deodar, mixed plantation, Teak mixed moist deciduous, and Pine mixed respectively, land confined in alpine pasture, sub-alpine fir, dry evergreen scrub, alpine scrub, scrub land as well as the terraced agriculture which available and provides visiting sites to the tourists.

There are various pasture land limits in the glacial and periglacial zone in the region.The upper parts of the Garhwal Himalaya have a exclusive flora and fauna diversity and also proposals massive probable for ecotourism for tourists, local community and researchers. It developed authoritative to take a stage to give more experience ecologically very rich diversity of the region among the world's tourism

society that paves the way to strengthen the economy and sustain the livelihood of local inhabitants of the region.

3.5 Data Acquisition

It is required to have at least two time periods of data to compare in order to monitor LULC changes. For assessing land use and land cover changes in any area, a remote sensing approach usually involves the use of satellite imagery from two or more dates. The imageries were chosen for this study based on their spatial resolution compatibility (30 m). Landsat data archives are sufficiently consistent with data from prior flights enable long-term regional and global LULC change to be assessed (Irons *et al.*, 2012). The cloud free Lansar-8 Thematic Operational Land Imager-OLI (30 meter spatial resolution) and thermal infrared sensor (TIRS) with two bands (band 10 and band 11 with 100 m resolution) (2015) images were used for analysing LULC change in the selected part of the Garwal region. These Lansat-8 images were downloaded from Earth Explorer website with no cost. The ArcGIS software was used for the preprocessing of the images like radiometric calibrations and atmospheric corrections were applied. However, the co-registeration of the images based on the sub-pixel accuracy was also carried out for removing geometric incongruity.

3.6 Remote Sensing as a Tool for Change Detection

Almost every day we can see that the surface of the earth is changing rapidly due to various reasons at local and regional scales with significant repercussions for people and for environment. To better understand, analyzing and predicting these changes, remote sensing satellite imagery are an unlimited basis of valuable material. The way scientists examine the atmosphere, seas, land, vegetation, glaciers, sea ice, and other environmental features of the Earth's surface has changed dramatically thanks to remote sensing satellite data from space The temporal resolution specifies the revisiting frequency of a satellite. Half a century of the satellite observations of the Earth have provided dramatic pictures and they are the basis for a new scientific paradigm: earth-system science (Tatem *et al.* 2008).

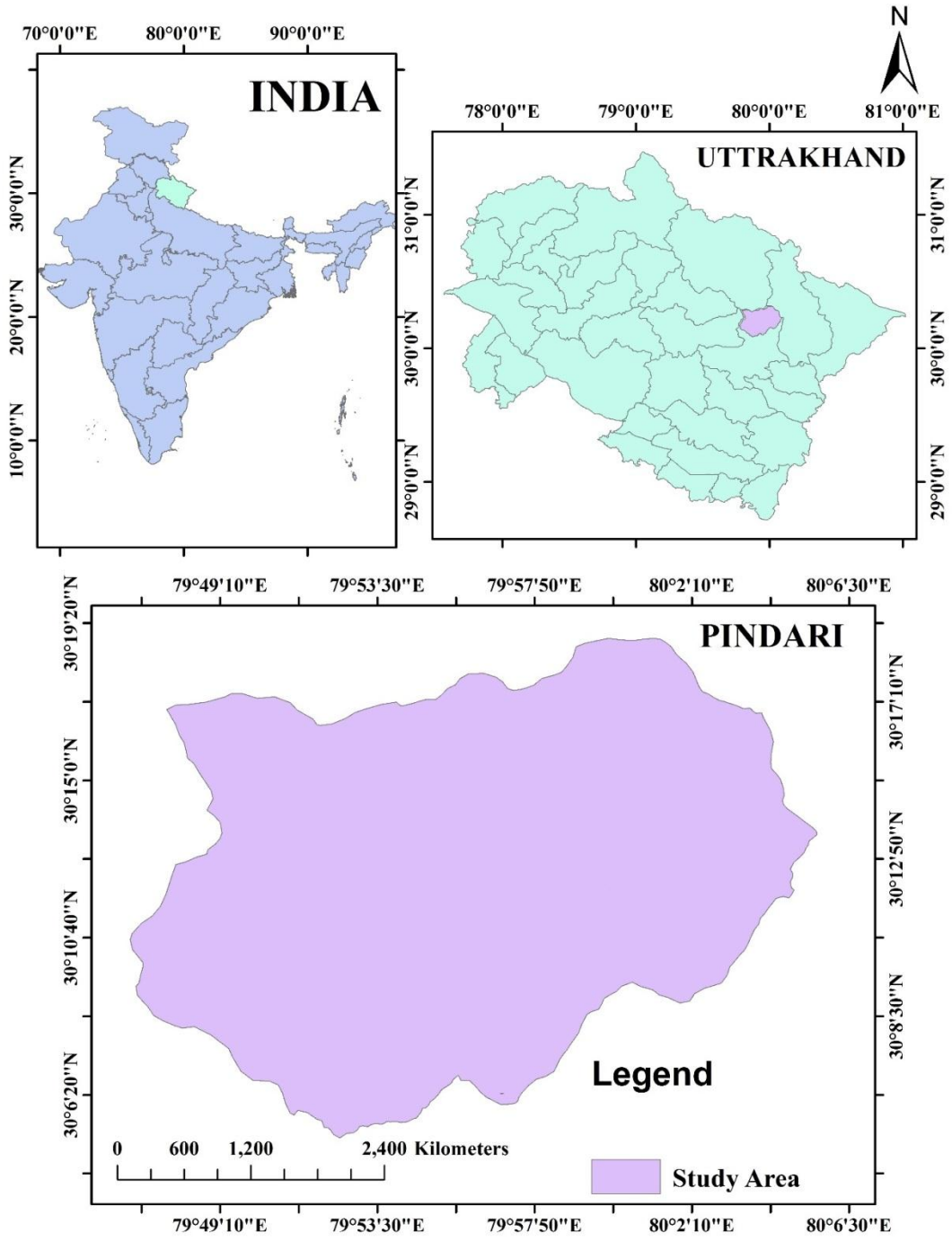

Figure 1: Study area

Congalton and Green (1999) note that the most basic remote sensing devices are the eyes and ears. There are many different ways to define remote sensing. One of the better explanations for remote sensing is: „Remote sensing is the science and the art of obtaining information about an object, area or phenomena through the analysis of data acquired by device that is not contact with the object, area or phenomena“ (Lillesand and Kiefer, 1994, pp. 1). A formal and comprehensive definition of applied remote sensing comes from Goddard Space Flight Centre, NASA, (URL 1).

The Canada Centre for Remote Sensing (CCRS 2007) defines distant sensing as follows: 'The science of receiving information near the Earth's surface without actually touching it is known as remote sensing. This is accomplished through detecting and recording reflected or emitted energy, as well as processing, evaluating, and applying that data ", In general, any way of seeing the Earth's surface without coming into close contact with it falls within the notion of remote sensing.

Remote sensing images have four different types of resolutions: spectral, spatial, radiometric and temporal (Jensen, 1996). Spatial resolution is limited by pixel size and refers to the size of the smallest object on the ground which means that the smallest resolvable object cannot be smaller than the pixel size. In this study all three series of the Landsat data images were re-sampled to the common nominal spatial resolution of 30 meters. Spectral resolution is defined as the number and wavelength of bands of electromagnetic energy detectable by a given sensor. A Landsat multispectral image consists of seven bands (green, red, near-IR bands, two SWIR bands and a thermal IR band). Each band represents an image acquired at a particular wavelength for band. The temporal resolution of a satellite sensor determines how often it returns to a certain place.

Remote sensing GIS and geospatial information systems are the two main components of geographic information science (GISci) (GIS). It also involves technologies such as the global positioning system (GPS), geodesy, and traditional mapping. (Goodchild 1992, Estes and Star, 1993, Hepner *et al*. 2005).The statement from twenty years ago „The integration of remotely sensed data (RS) and geographic information system (GIS) technology is one of the great ideas whose time has

come"(Faust *et al*. 1991) is today extremely relevant, while the another statement from that year „Remotely sensed images have been shown to be a cost effective means for update GIS data"(Faust *et al*. 1991) is today clearly demonstrable. Today RS, GIS, GPS, spatial analyses and data visualisations are a central part of the LULC characterization and analysis. There are many studies dealing with the remote sensing and GIS data integration (Ehlers 1991, Lauer *et al*. 1991, Hinton 1996, Tsou 2004, Merchant and Narumali, 2010). Rogan and Miller (2006) outlined four methods for combining GIS and remote sensing data:

(1) GIS can be used to manage multiple data types,

(2) GIS analysis and processing methods can be used for manipulation and analysis of remotely sensed data (e.g. neighbourhood or reclassification operations),

(3) Remotely sensed data can be manipulated to derive GIS data, and

(4) GIS data can be used to guide image analysis to extract more complete and accurate information from spectral data. Remote sensing in conjunction with Geographical Information Systems (GIS), because of its ability to interrelate multiple types of various information and data obtained from a range of source, has been widely recognized as powerful tools to derive accurate and timely information on the spatial distribution of LULC changes.

3.7 Software Used (ARCGIS) 10.3

The methodology for on screen interpretation of multi data satellite data comprises the following six major steps.

1. Section and acquisition of data.
2. Preliminary on screen interpretation.
3. Ground data collection and verification
4. Final interpretation and modification.
5. Area estimation.
6. Final thematic map preparation.

Due to the mountainous topography of the study area, image preprocessing of the satellite images was necessary to reduce or eliminate differences between the two dates due to atmospheric or sensor variations. For geometric registration , the images of two decades 2010 and 2020 been taken.

3.7.1 Classification criteria

The following criteria should be met by a land use and land cover categorization system that can effectively use orbital and high-altitude remote sensor data. (Anderson, 1971) :

1. The accuracy of distant sensor data interpretation of land use and land cover categories should be at least 85%.
2. The accuracy of interpretation for the several categories should be about equal.
3. From one interpreter to the next, and from one sensing time to the next, repeatable or recurring outcomes should be possible.
4. The classification system should be applicable over extensive areas.
5. The classification should allow for the use of plants and other types of land cover as activity surrogates.
6. The categorization system should be able to work with data from remote sensors collected at various periods throughout the year.
7. It should be possible to make effective use of subcategories derived from ground surveys or from the use of bigger scale or upgraded remote sensor data.
8. Aggregation of categories must be possible.
9. Comparison with future land use data should be possible.
10. Multiple uses of land should be recognized when possible.

A classification scheme was developed based on ancillary information. The visual interpretation was completed using ARCGIS to obtain a training set for each class that was completely based on Google earth. In addition, unsupervised classification and NDVI (Normalized Difference Vegetation Index) determination

were also applied before the supervised classification to aid in the identification of dominant land-cover types and improve the classification accuracy. Then, supervised classifications using the maximum likelihood method were performed in GOOGLE IMAGINE for the 2010 and 2020. Landsat images. Based on a visual inspection of the locations on Google Earth and the picture itself, 75-85 ground-truth polygons were scanned for each class. Training polygons with perplexing spectral signatures were deleted, and new ones were produced based on a visual inspection of the locations on Google Earth and the image itself. The maximum likelihood method was then ran one again. The identified six to eight land cover classes included dense forest, vegetative land, zero land, green land, waste land, water bodies, and snow and glacier.

3.7.2 Land-cover classification scheme

Table 1 : Land-cover classification scheme

Land Cover	Description
Dense forest	'Dense forests' are defined as those where the tree canopy density is 70 per cent or above; 'moderately dense forests' have been defined as areas with tree canopy density between 40 to 70 per cent and 'open forest area' is when the canopy density is between 10 to 40 per cent.
Vegetative land	These areas have distinct types of plants, soil, and weather patterns. Vegetation regions can be divided into five major types: forest, grassland, tundra, desert, and ice sheet
Waste land	An area of land that cannot be used or that is no longer used for building or growing things on
Water bodies	A body of water forming a physiographical feature, for example a sea or a reservoir.
Snow	Small, soft, white pieces of frozen water that fall from the sky in cold weather
Glacier	A mass of ice that moves slowly down a valley

Accuracy assessment is important in validating the digitally classified images. It is the procedure used to compare the classification results to the geographical reference data that are assumed to be true. Due to the mountainous topography of the

study area, ground reference data were collected from Google Earth with limited ground GPS points. , An accuracy assessment was performed with 2010 and 2020 with Google Earth image archive.

3.7.3 Land-Use and Land-Cover (LULC) Change Analysis

In ArcGIS [10.3], a cross-tabulation module detection approach was employed to identify land-use and land-cover change (LULC), resulting in a LULC change matrix. This matrix contains crucial data on the nature and spatial distribution of land use changes. The major sorts of changes or directions in the research region may be identified using a change matrix. Then, the change in LULC was analyzed to depict gains and losses for the two time periods. The gains and losses for land-cover categories were likewise driven by the change matrices of the first period (2000) and the second period (2020). The gains and losses for each class were calculated by subtracting the persistence from the column total and removing the persistence from the row total, respectively.

3.8 Procedure of sebal model for LST computation

The Landsat-8 satellite having two types of the sensors namely Operational Land Imager (OLI) and Thermal Infrared Sensors (TIRS). Onboard Landsat-8 is the Operational Land Imager (OLI), which generates 9 spectral bands (Band 1 to 9). OLI pictures can distinguish between different vegetation types, cultural traits, biomass, and vigour, among other things. The Thermal Infrared Sensor (TIRS) is made up of two thermal bands with a 100-meter spatial resolution. TIRS is a technique for measuring the thermal energy of the Earth that is particularly valuable for tracking how land and water are used.

Temperature data is collected by the Landsat 8 TIRS sensors and stored as a digital number (DN) with a range of 0 to 255. The following is a detailed step-by-step technique for calculating Land Surface Temperature (LST).

To compute the corrected thermal radiance, first calculate the emissivity in the thermal band, which requires the spectral radiance (L_λ), reflectivity values in each band (ρ_λ), and the surface albedo (ε).

3.8.1 Computation of spectral radiance (L_λ)

The spectral radiance is the radiant energy detected by satellite sensors at the top of the atmosphere. Using the formula below, we estimated the spectral radiance for each band(Waters *et al.*, 2002).

$$L_\lambda = \frac{L_{\max} - L_{\min}}{65535} DN + B$$

Where, L_λ is spectral radiance in W/m^2/srad/Hz and DN value represents the degree of greyness of the pixels. $L_{\max}$ and $L_{\min}$ are the maximum and minimum values of spectral radiance observed the sensor (in W/m^2/srad/Hz) for each band. Table shows the maximum and minimum detactable values of the of the spectral radiance by sensor along with the ESUN values for Landsat-8 sensors, as shown in (Table 2),

Table 2. Metadata of the Landsat 8 image for maximum and minimum spectral radiance along with the ESUN for each band

Band No.	Maximum radiance	Minimum radiance	ESUN
1	741.76410	-61.25512	2027
2	759.57544	-62.72599	2067
3	699.94232	-57.80146	1893
4	590.23077	-48.74145	1603
5	361.19180	-29.82734	972.6
6	89.82511	-7.41779	245
7	30.27587	-2.50019	79.72
8	667.97882	-55.16191	-
9	141.16194	-11.65720	399.7
10	22.00180	0.10033	-
11	22.00180	0.10033	-

3.8.2 Computation of Reflectivity (ρ_λ)

The ratio of reflected energy to the quantity of energy impacting the surface is the reflectivity of a surface. The following formula (Waters *et al.*, 2002) is used to compute the amount of reflection for each band,

$$\rho_\lambda = \frac{\pi . L_\lambda}{ESUN_\lambda . \cos\theta . d_r}$$

Where, ρ_λ is stand for the spectral reflectivity, $ESUN_\lambda$ is the average solar radiation over TOA in W/m^2/mm. θ is the the incident angle of the sun's radiation and computed as,

$$\theta = 90 - \beta$$

β is the sun's elevation angle can be find from the header file of the Landsat satellite image provided in every scene. It depends on the geographical locations.

The Duffie and Beckman(1980) formula is used for the computation of the inverse of the square distance between the Earth and the sun (d_r) as,

$$d_r = 1 + 0.033 . \cos\left(DOY \frac{2\pi}{365} \right)$$

Where, DOY represents the day of year in the sequential manner of the calender.

3.8.3 Computation of surface radiation (ε)

The ratio between thermal energy emitted from a surface and blackbody is known as surface radiation. In the SEBAL method, there are two surface radiations are employed namely thermal energy emitted in a narrow thermal band (εNB) of 10.5 to 12.5 microns, and thermal energy emitted in a broad band ranges ($\varepsilon 0$) 6 to 14 microns. The following assumption has been taken in our study,

For the NDVI greater than zero, following two conditions are applied as,

(a) LAI < 3,

$$\varepsilon NB = 0.97 + 0.0033 \times LAI$$

$$\varepsilon 0 = 0.95 + 0.01 \times LAI$$

(b) LAI > 3

$$\varepsilon NB = 0.98$$

$$\varepsilon 0 = 0.98$$

For water and snow, the values of εNB and $\varepsilon 0$ are used as,

Water:

NDVI< 0; $\alpha < 0.47$: $\varepsilon NB = 0.99, \varepsilon 0 = 0.985$

Snow:

NDVI< 0; $\alpha > 0.47$: $\varepsilon NB = 0.99, \varepsilon 0 = 0.985$

Here, α represents the surface albedo.

3.8.4 Computation of brightness temperature (T_B)

The microwave radiation radiance going upward from the top of the Earth's atmosphere is known as brightness temperature (TB). The following equation is used to compute the brightness temperature,

$$T_B = \frac{k_2}{\ln\left(\frac{k_1}{L_{11}}\right)}$$

Where, k1 and k2 are the thermal band's spectral radiance. The resulting k1 and k2 values were 480.89 and 1201.14, respectively, with L11 being the spectral brightness of band 11.

3.8.5 Computaion of Land surface tempearature (T_s)

The computation of Land Surface Tempearature (LST) is carried out by the given formula,

$$T_s = \frac{T_B}{\varepsilon NB^{0.25}}$$

Where, T_B is the brightness temperature, and εNB is the emissivity of narrow band surfaces.

3.9 Establishment of relationships between estimated and predicted LST's

The average pixel value of (3×3 pixel) modified species diversity indices were extracted and correlated by using ground control points of training samples plots. Linear regression was accomplished to model for the relationship between species diversity indices and remotely sensed data obtained by SAR and Optical imagery.

To evaluate and validate the performance of models that employed in the study are generated by using in-situ measure and machine learning developed predictor model of DIs value (Le Moan *et al.*, 2011).

SVM (linear, polynomial, radial, sigmoid) and RF supervised machine learning algorithm model has been employed for the retrieval tree species diversity by using various input parameters. Various metrics are also used to measure the operations of the models, such as coefficient of correlation (r), Root Mean Square Error (RMSE), and Bias. These metrics were employed to evaluate and measure the accuracy of the model and essentials for the comparative analysis of various models. The coefficient of correlation (r) is used to calculate that how two different variables are linearly related with each other, and mathematically it is stated as follows:

$$r_{xy} = \frac{\sum_{i=1}^{n}\left(x_i - \underline{x}\right)\left(y_i - \underline{y}\right)}{\sqrt{\sum_{i=1}^{n}\left(x_i - \underline{x}\right)^2}\ \sqrt{\sum_{i=1}^{n}(y_i - y)^2}} \quad \ldots\ldots\ldots\ldots\ldots\ldots(1)$$

Where, n represents the number of samples, x_i and y_i are the i^{th} sample of parameters x and y and $\underline{x} = \frac{1}{n}\sum_{i=1}^{n} x_i$ is the mean value of the sample (similarly applied for $\underline{y}$). The value of r varies from -1 to +1, and where the -ve value denoted the negative correlation in contrast +ve values represent a positive correlation between those two different variables.

The Root Mean Square Error (RMSE) is generally used to evaluate the averaged magnitude of error between the observed and predicted samples set. It is mainly the square root of the average of the squared difference between observed and predicted samples set and it can be mathematically expressed as:

$$RMSE = \sqrt{\frac{1}{n}\sum_{i=1}^{n}(y_i - \acute{y}_i)^2} \qquad \text{.....(2)}$$

Where, n represents the sample number, y_i is the observed i^{th} sample and $\acute{y}$ is the predicted value of the sample at the i^{th} position. RMSE value is always non-negative in which value 0 denotes a perfect fit for the evaluation.

Bias is applied for the estimation of the mean error in a sample set of predictions without taking into consideration their direction. It can be expressed as:

$$Bais = \frac{1}{n}\sum_{i=1}^{n}(y_i - \acute{y}_i) \qquad \text{.....(3)}$$

CHAPTER 4

RESULTS AND DISCUSSION

4.1 Preprocessing and Landsat Band Statistics

We must first execute a preprocessing procedures, including atmospheric correction, cloud and cloud shadow identification, and composite/fusion/metrics, before applying change detection algorithms. Most of the change detection methods only use Level 1 terrain-corrected Landsat images pictures as inputs. Geometric correction is often deemed unnecessary if just landsat images are used in change detection because the landsat images have high geometric accuracies(Zhu and Woodcock, 2014). The band statisctics are computed for the Landsat images of the years 2000 and 2020 to ensure the good quality of the data achived after the preprocessing. Figure 4.1 and 4.2 show the band statistics of the Landsat images for the years 2000 and 2020, respectively.

4.2 Estimation of Land Surface Temperature using SEBAL method

The procedure for the estimation of the Land Surface Tempearature using the SEBEL method is given in the above section 3.8. The axullary data for the computation of LST using SEBAL provided in Figures 4.3 to 4.14 for the years 2000 and 2020, respectively. Figures 2 and 3 show the spatial distribution of the albedo over the study for the year 2000 and 2020, respectively.

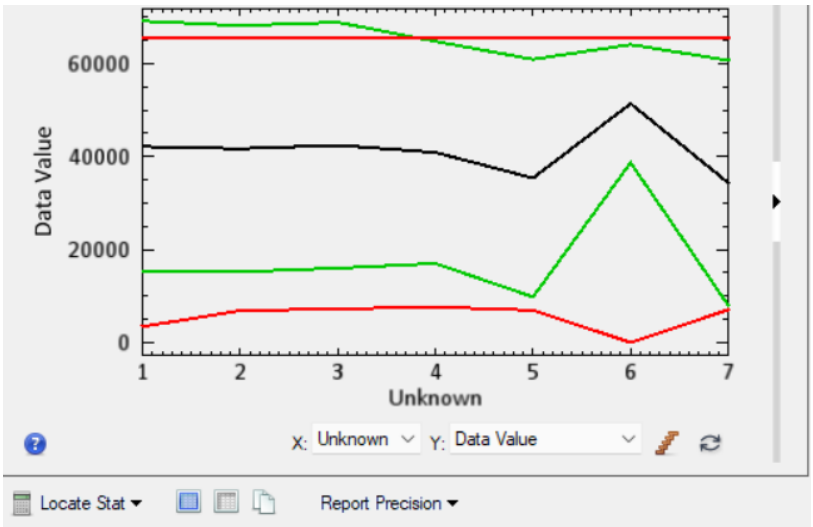

Locate Stat ▾ Report Precision ▾

Basic Stats	Min	Max	Mean	StdDev
Band 1	3406	65536	42155.619632	27019.562497
Band 2	6848	65536	41705.424572	26499.466834
Band 3	7236	65536	42450.162798	26452.515030
Band 4	7621	65536	40899.187214	23900.046291
Band 5	6930	65536	35372.126291	25573.147328
Band 6	0	65536	51402.408742	12704.165867
Band 7	7034	65536	34363.927590	26365.606436

Figure 2. Band statistics of Landsat image for the year 2000

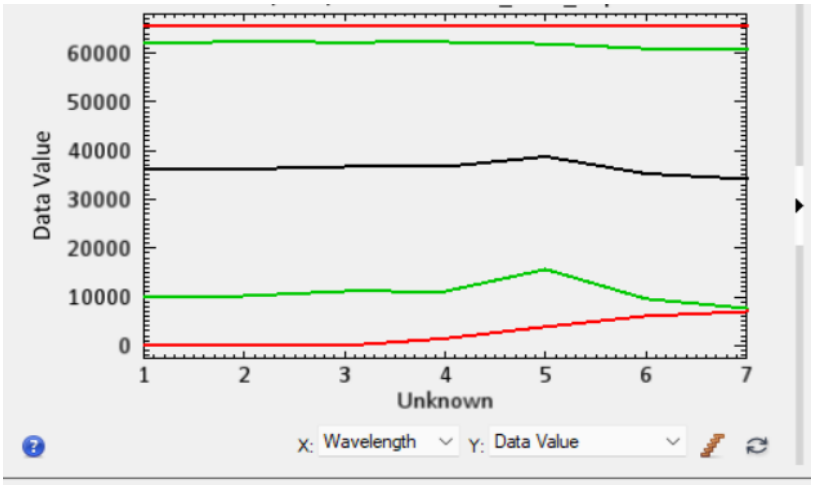

Locate Stat ▾ Report Precision ▾

Basic Stats	Min	Max	Mean	StdDev
Band 1	1	65536	36083.771298	26149.655233
Band 2	1	65536	36239.832844	26051.362776
Band 3	4	65536	36707.876830	25556.348289
Band 4	1454	65536	36712.778944	25577.303279
Band 5	3876	65536	38780.658793	23132.675647
Band 6	6061	65536	35275.134556	25670.030752
Band 7	6995	65536	34178.903058	26529.212802

Figure 3. Band statistics of Landsat image for the year 2020

Albedo is a crucial parameter used for the land surface energy balance studies. The remote sensing techniques is widly for to map land surface albedo on regional and global scales. It defined as the proportion of the incident engery or energy radiated from the land surface. Recently fallen snow reflects the maximum incoming solar radiation, indicates the high value of albedo in between 0.96 to 0.98 for visible and near-UV range radiation and average 0.8 for the entire range of solar radiation(Grenfell *et al.*, 1994). The snowpack has lower albedo causes it absorbs more incoming radiation, which is responsible for heating of the land surface(Warren, 1982). The pictorial representation of spatial distributed albedo values fallen in the year 2020 with respect of the year 2000. It is clearly indicated that the land surface become hoter in 2020 than 2000. Figures 4 and 5 show the spatial distribution of the emmisivity over the study for the year 2000 and 2020, respectively.Emissivity defined as the amount of the radiated energy from the land surface in comparision to the black body. The land surface emissivity is highly correlated to the normalized difference vegetation index (Sobrino *et al.*, 2008; Van de Griend and OWE, 1993). The higher values of the emissivity is found in the year 2020 in comparison of the year 2000 over some portion of study area by the pictorial representation. It clearly indicates that the land surface absorbs more in the year of 2020 in the comparison of the year 2000. It also responsible for the increasing land surface tempearature(Anand *et al.*, 2021; Ball and Pinkerton, 2006; Jenerette *et al.*, 2016; Kimball, 2005; Mackay and Matsugu, 1973; Mildrexler *et al.*, 2011; Setiawan and Masitah, 2017).

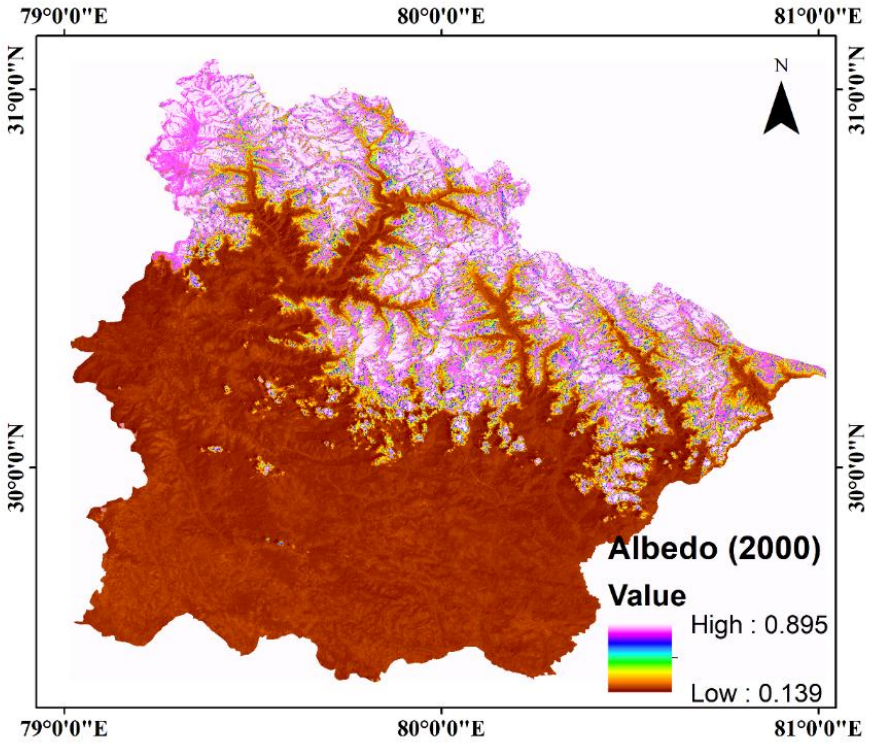

Figure 4. Albedo map for the year 2000 over the study area

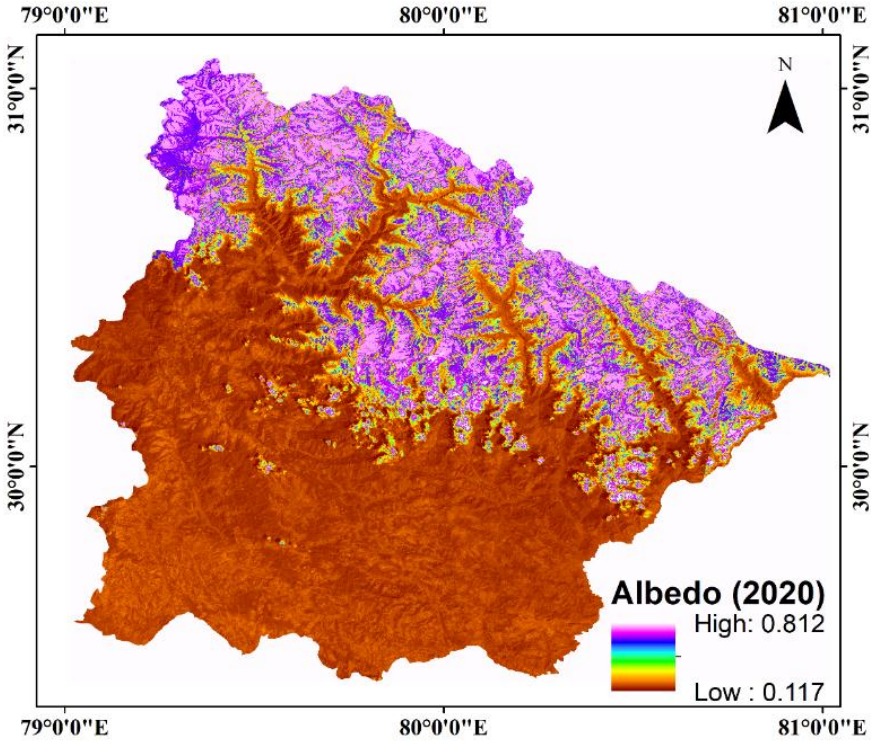

Figure 5. Albedo map for the year 2020 over the study area

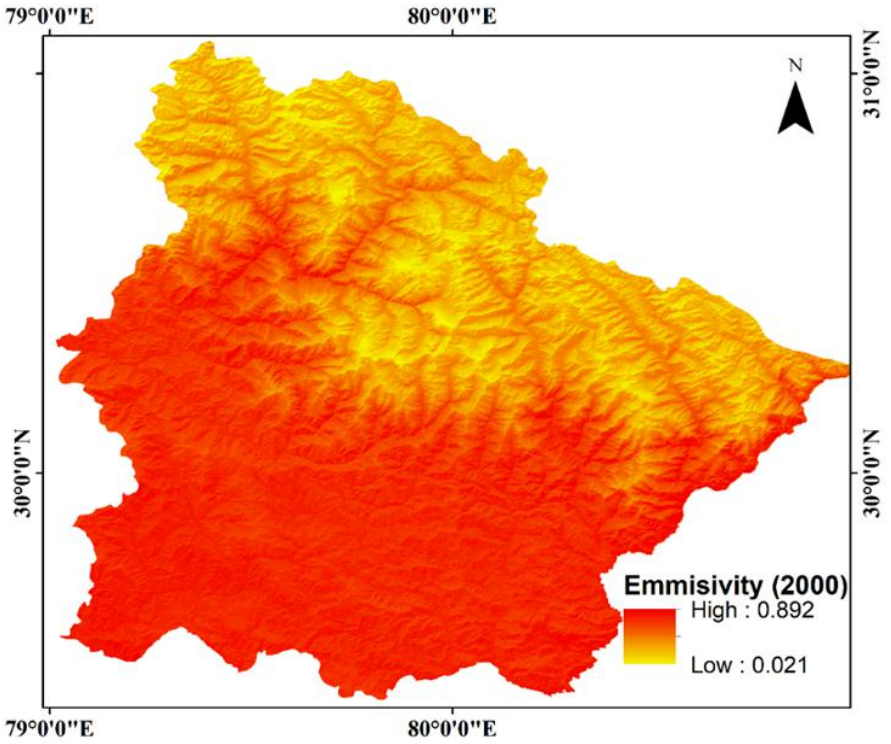

Figure 6. Emissivity map for the year 2000 over the study area

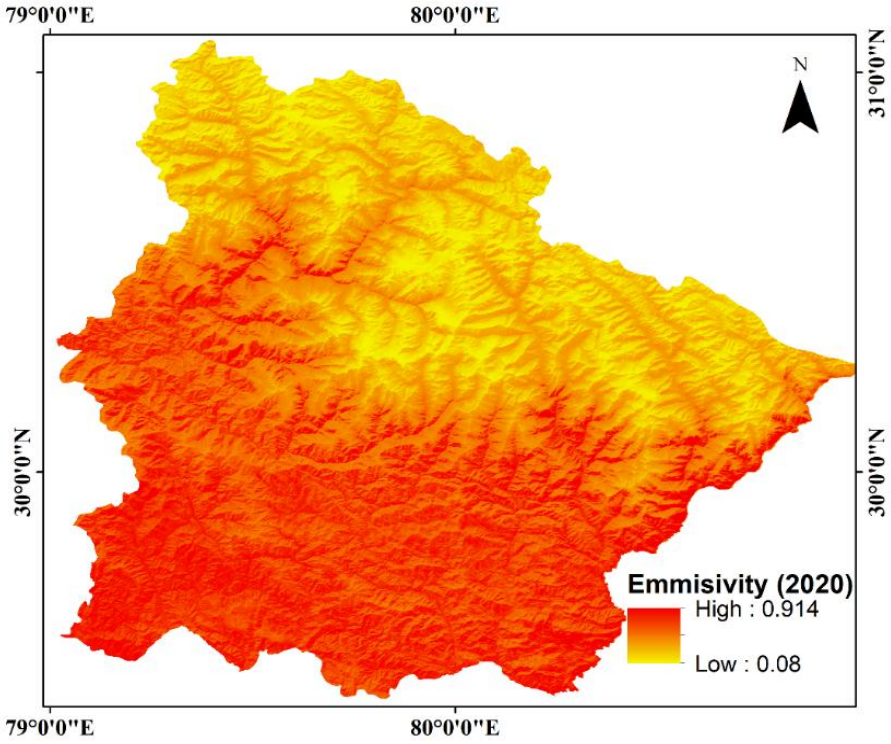

Figure 7. Emissivity map for the year 2020 over the study area

Figures 8 and 9 show the spatial distribution of the leaf area index (LAI) over the study for the year 2000 and 2020, respectively. The ratio between the amount of one sided leaf area with the ground surface area is measured by the leaf area index(Breda, 2003; Chen and Black, 1992; Chen *et al.*, 1997; Myneni *et al.*, 1997). The LAI paly an very crucial role for the understanding terrestrial ecological, hydrological, and biogeochemical processes (Andersen *et al.*, 2002; de Almeida *et al.*, 2019; Kergoat, 1998; Nemani *et al.*, 1993; Ryu *et al.*, 2010). LAI can be calculated using statistical or physical approaches from remote sensing data. The empirical association between the LAI and surface reflectance or vegetation indices is used in the statistical approaches. Figures 10 and 11 show the spatial distribution of the (SAVI) over the study for the year 2000 and 2020, respectively (Gilabert *et al.*, 2002; Huete, 1988; Rondeaux *et al.*, 1996). The influences due to the soil brightness emission in the retrieval of NDVI values is compensated by using SAVI over the low vegetation cover(Ren *et al.*, 2018; Venancio *et al.*, 2019). SAVI produced from Landsat Surface Reflectance is estimated as a ratio of R and NIR values with a soil brightness correction factor (L) of 0.5 to account for most land cover types(Jiang *et al.*, 2007). The pictorial representation for the changes in SAVI during the time period years 2000 to 2020, can be clearly seen. It showed the value of SAVI increases in the glacier portion of the study area in year 2020 in comparison of the year 2000. It indicates that the some impurities are induced over the glacier during this time period, which is responsible for the degredation of glacier.

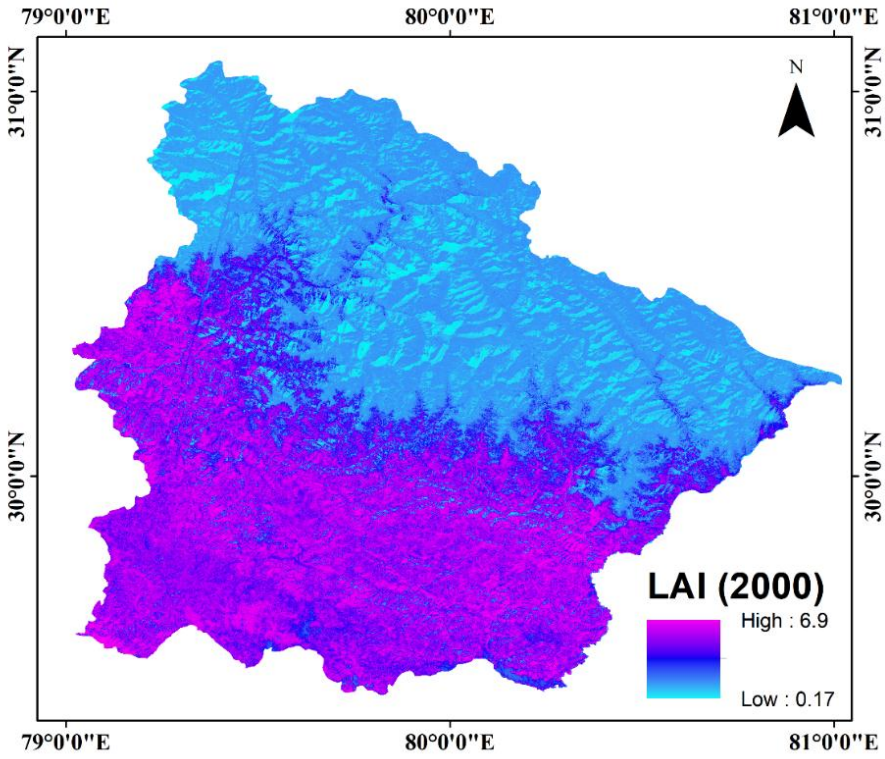

Figure 8. Leaf area index map for the year 2000 over the study area

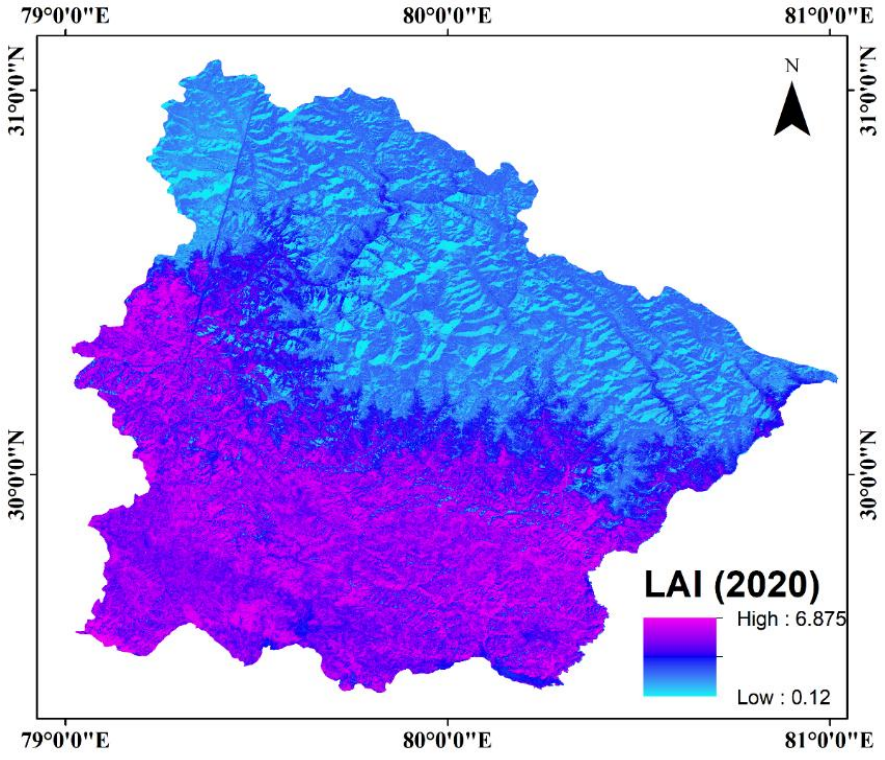

Figure 9 Leaf area index map for the year 2020 over the study area

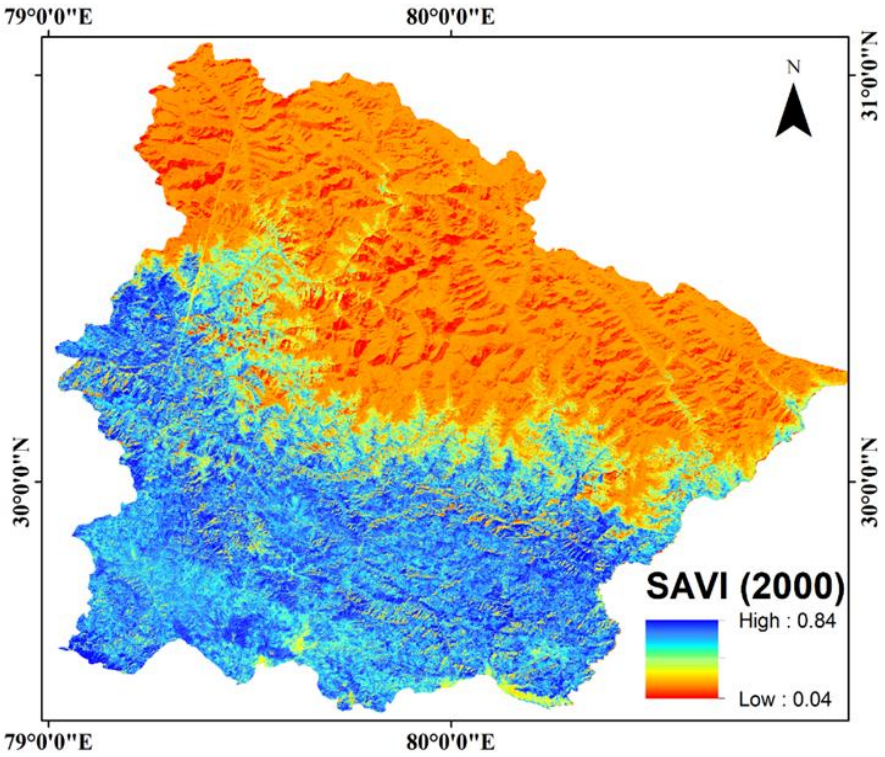

Figure 10. SAVI map for the year 2000 over the study area

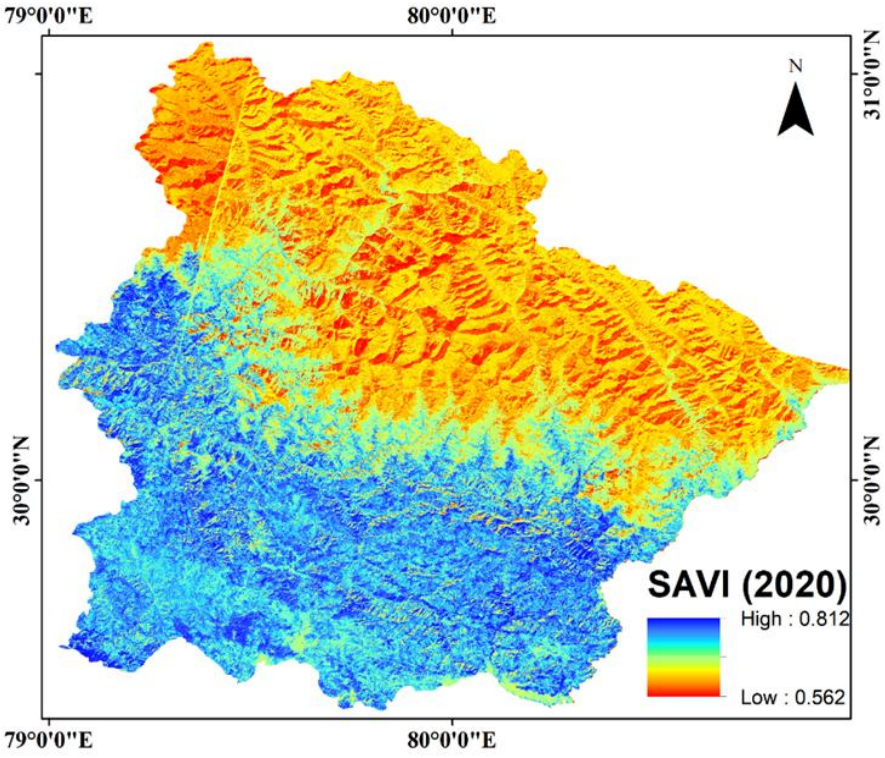

Figure 11. SAVI map for the year 2020 over the study area

Figures 12 and 13 show the spatial distribution of the Normalized Difference Vegetation Index (NDVI) over the study for the year 2000 and 2020, respectively. NDVI is the common vegetation index, which is widely used in many ecosystem and environmental applications. NDVI is computed as the ratio between TOA reflectance of a red band and near-infrared band(Carlson and Ripley, 1997; Chen *et al.*, 2004; Tucker *et al.*, 2005). A heavily vegetated area's NDVI will incline toward positive readings, whereas water and built-up areas' NDVI will be near 0 or negative(Gamon *et al.*, 1995; Pettorelli *et al.*, 2005). The drought condition is strongly linked with the satellite derived NDVI. The varied wavelengths of visible and near-infrared sunlight reflected by the plants are studied to determine the density of green on a patch of land(Hu *et al.*, 2019; Patel *et al.*, 2012; Wan *et al.*, 2004). Low red-light reflectance and high near-infrared reflectance characterise healthy vegetation, resulting in high NDVI values. Positive NDVI values are increasing, indicating an increase in the amount of green vegetation. Nonvegetated characteristics, such as barren surfaces (rock and soil), water, snow, ice, and clouds, are indicated by NDVI values near 0 and decreasing negative values(Basso *et al.*, 2004; Morgan *et al.*, 2021; Recio *et al.*, 2012; Zaitunah and Sahara, 2021). Figures 14 and 15 show the spatial distrubition of land surface tempeartures over the study area for the year 2000 and 2020, respectively. This land surface temperature is computed using the Landsat satellite data by SEBAL method(Chang *et al.*, 2017; Jaafar and Ahmad, 2020; Kamran *et al.*, 2015; Li and Zhao, 2010). The pectorial representation of LST during two different years 2000 and 2020 are clearly observed.

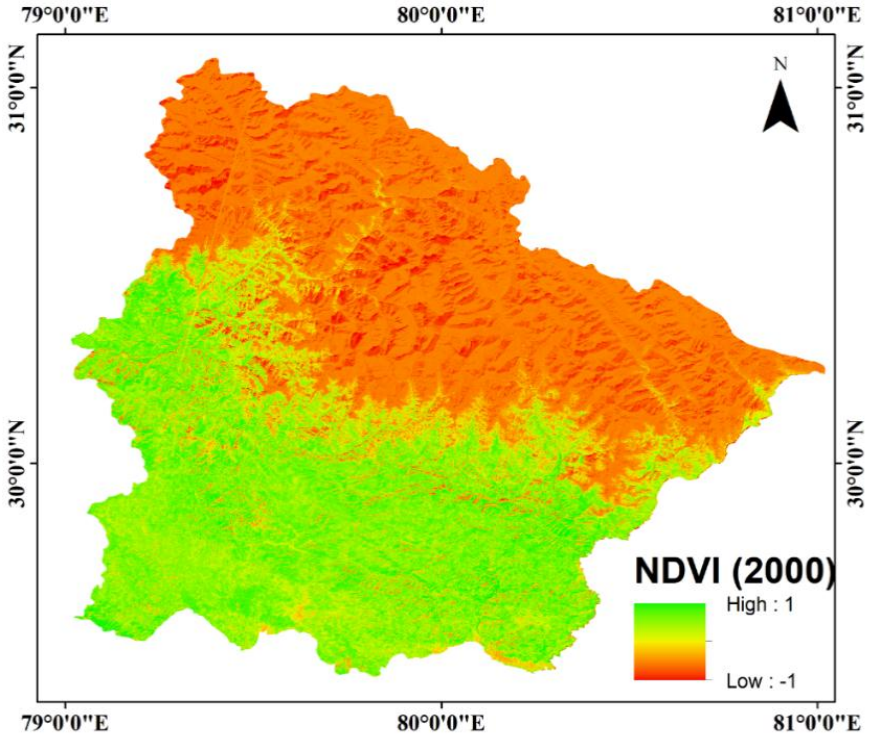

Figure 12. Normalized difference vegetation index map for the year 2000 over the study area

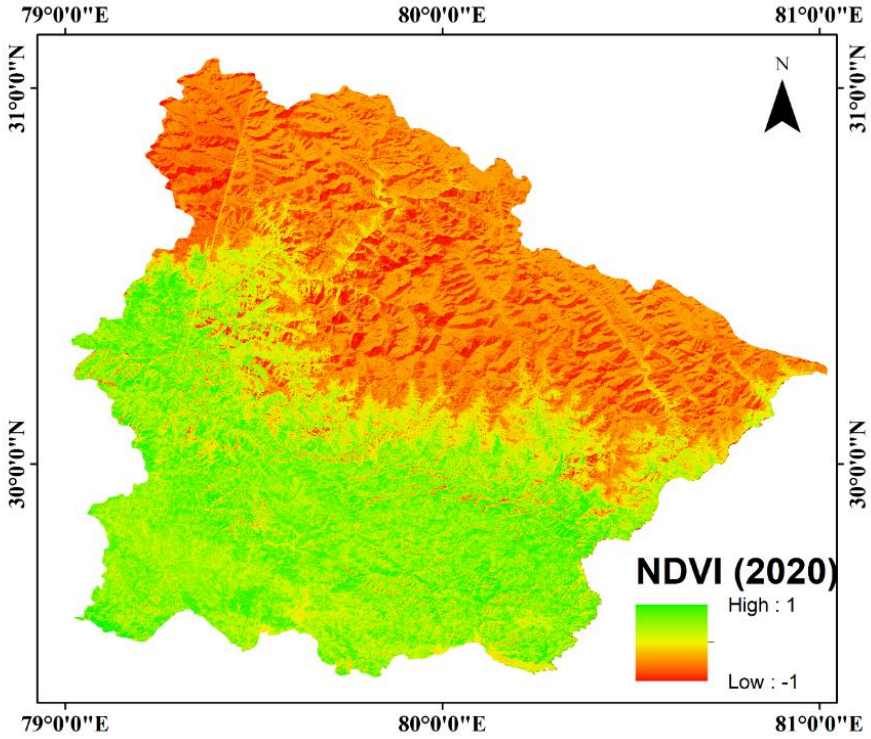

Figure 13. Normalized difference vegetation index map for the year 2020 over the study area

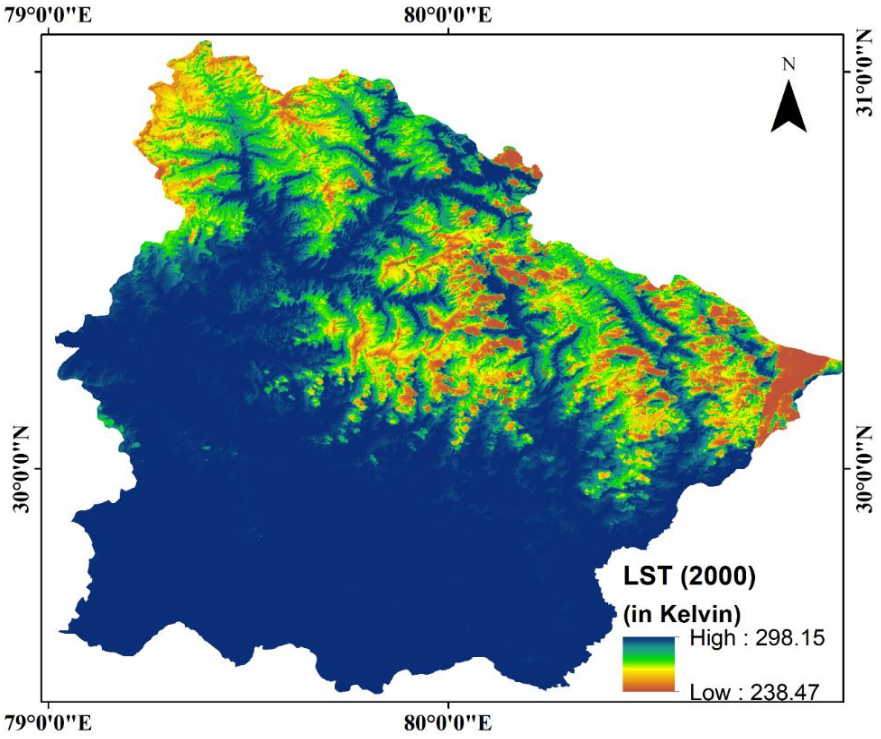

Figure 14. Land surface temperature map for the year 2000 over the study area

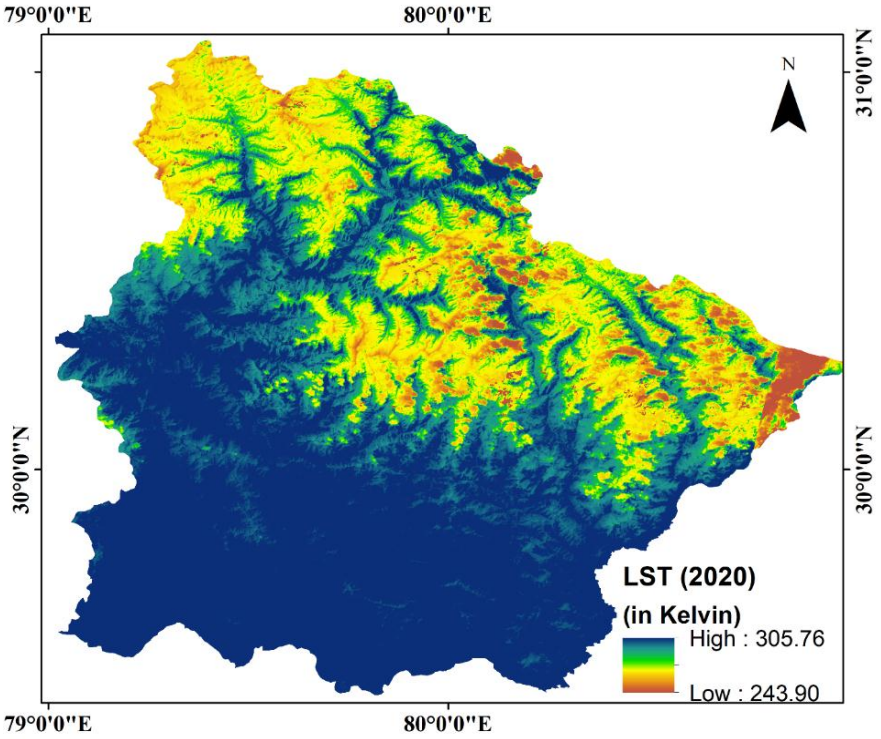

Figure 15. Land surface temperature map for the year 2020 over the study area

4.3 Land-Use and Land-Cover (LULC) Change

The land use land cover (LULC) changes mapping in the Himalayas region are regulary carried out by many researchers and scientist for long-term development, planning, and management(Dorji *et al*., 2014; Garrard *et al*., 2016; Ishtiaque *et al*., 2017; Mishra *et al*., 2020; Munsi *et al*., 2010; Rasool *et al*., 2021; Roy and Das, 2021; Ullah *et al*., 2019). The present study uses remote sensing and geographic information system techniques for LULC mapping over the Grwal region most specifically Pindari to track changes from the year 2000 to 2020. Figure 4.16 and 4.17 show the land cover maps for the year 2000 and 2020 are based on Landsat 8 (OLI) satellite data were prepared with five land-cover types, namely, Dense forest, Open forest, Agriculture fields, Waste land, and Snow/Glacier. The final output of the supervised classification, which consists of two classified maps of the Garhwal region and a comparison in terms of the total area for each land cover category. The LULC maps for 2000 and 2020 are mentioned where Some changes can be captured by comparing the maps visually.

The area occupied retrieved from the classified maps indicated that in the year 2000 in different classes viz; Dense forest was about 6618.874 (in square km), Open forest was 4808.34(in square km), Agricultural land area covered 2845.37(in square km), Wasteland covered the area 1766.03(in square km) and Snow/Glacier occupied about area 7927.56 (in square km), respectively. However, the Dense forest was about 5545.05 (in square km), Open forest was 4903.7 (in square km), Agricultural land area covered 2802.16 (in square km), Wasteland covered the area 1646.08 (in square km) and Snow/Glacier occupied about area 9078.09 (in square km), respectively for the year 2020. These values are also provided in Table 4.1 and Figure 4.17.

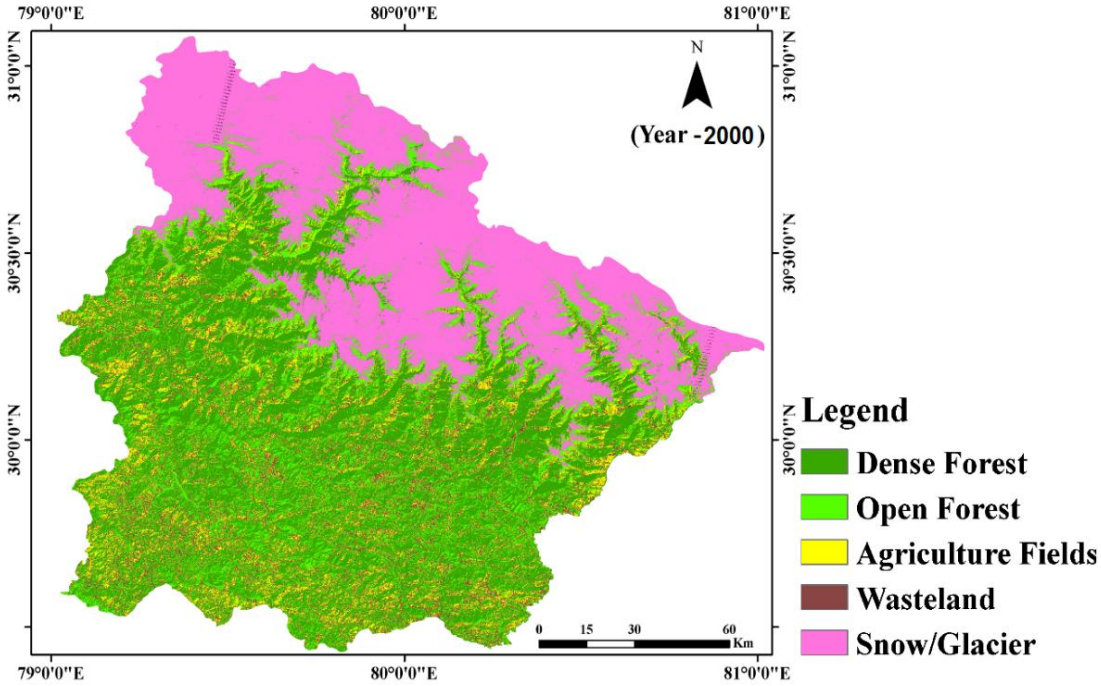

Figure 4.16. Classified map for the year 2000 in five different classes like dense forest, open forest, agricultural filed, wasteland and snow/glacier

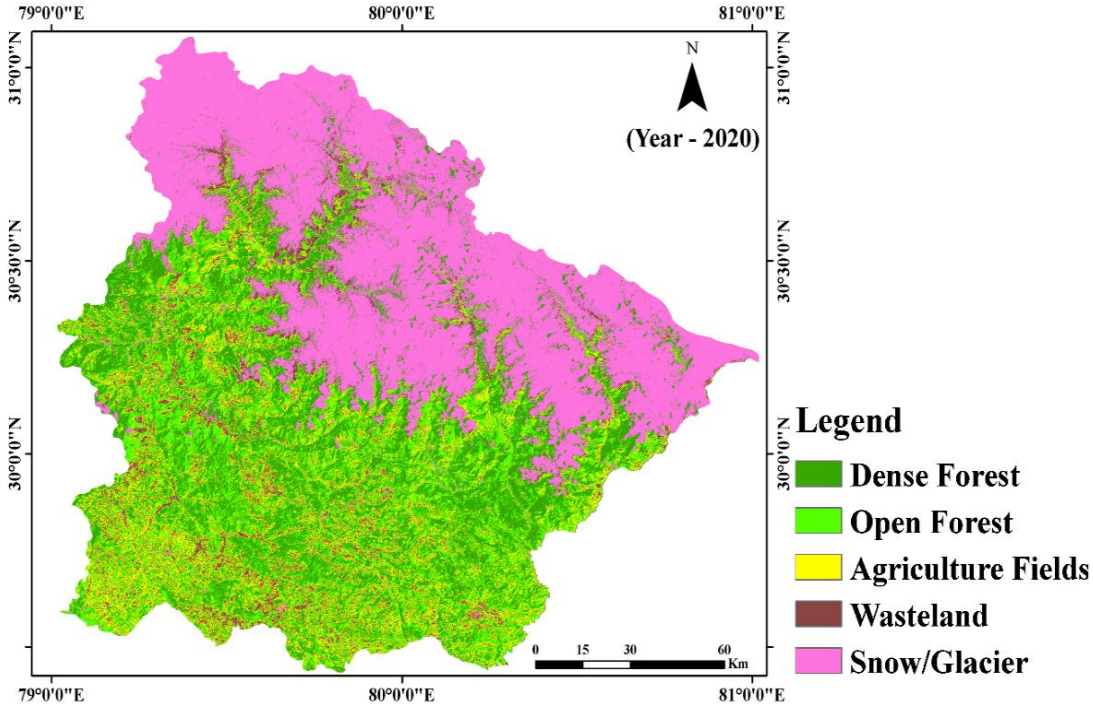

Figure 4.17. Classified map for the year 2020 in five different classes like dense forest, open forest, agricultural filed, wasteland and snow/glacier

Outcomes from the classified maps of the year 2000 illustrate that the Dense Forest, Open Forest, Agriculture Fields, Wasteland, and Snow/Glacier covered the area about 27.618%, 20.063%, 11.872%, 7.369% and 33.078%, respectively. However, Dense Forest, Open Forest, Agriculture Fields, Wasteland, and Snow/Glacier covered the area about 23.128%, 20.453%, 11.688%, 6.866% and 37.865%, respectively for year 2020.

Table 3: Area calculation for LU/LC feature classes

Classes	Year 2000		Year 2020		Area change in sq.km	Area change in %
	Area in sq.km	Area (%)	Area in sq.km	Area (%)		
Dense Forest	6618.874	27.618	5545.050	23.128	-1073.824	-4.49
Open Forest	4808.34	20.063	4903.700	20.453	95.36	0.39
Agriculture Fields	2845.37	11.872	2802.160	11.688	-43.21	-0.184
Wasteland	1766.03	7.369	1646.080	6.866	-119.95	-0.503
Snow/Glacier	7927.56	33.078	9078.090	37.865	1150.53	4.787

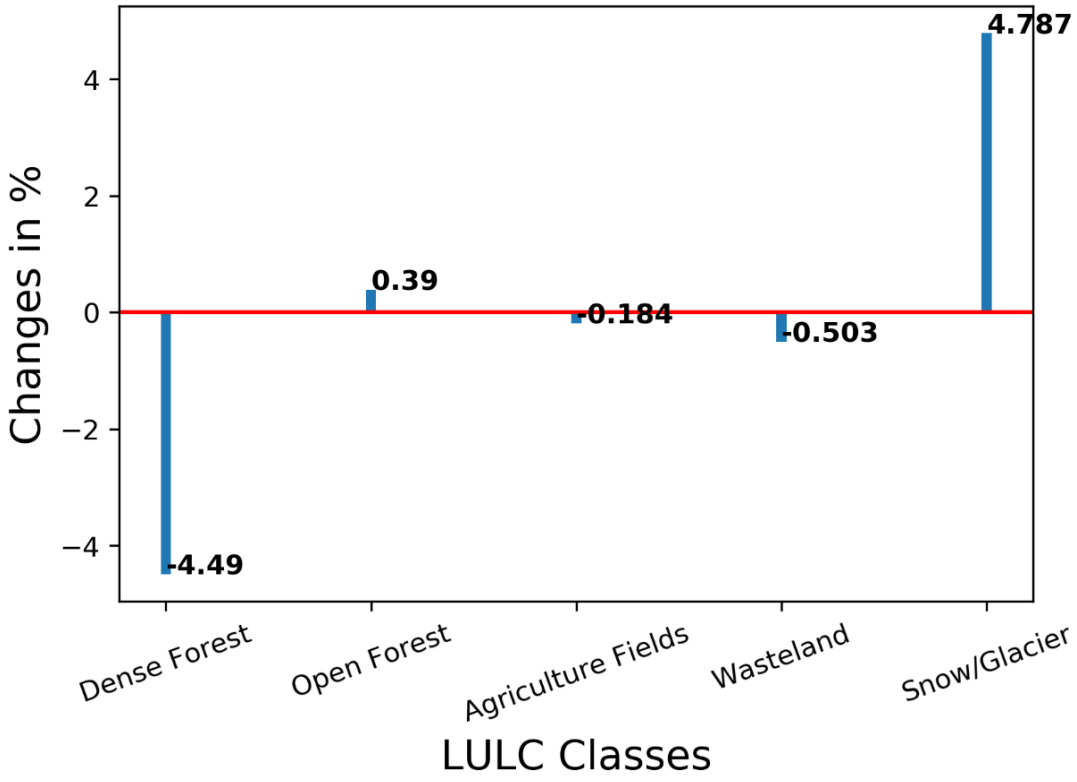

Figure 4.18. Percentage changes in various land cover classes form the year 2000 to 2020

Table 4: Confusion Matrix for LU/LC of Year 2000

Class	Dense Forest	Open Forest	Agriculture Fields	Wasteland	Snow/Glacier	Total	User's Accuracy (%)
Dense Forest	50	0	10	0	0	60	83.33
Open Forest	0	50	0	0	0	50	100
Agriculture Fields	0	0	40	0	0	40	100
Wasteland	0	0	0	50	0	50	100
Snow/Glacier	0	0	0	0	50	50	100
Total	50	50	50	50	50	250	
Producer's Accuracy (%)	100	100	80	100	100		
						Overall Accuracy (%)	95

Table 5: Confusion Matrix for LU/LC of Year 2020

Class	Dense Forest	Open Forest	Agriculture Fields	Wasteland	Snow/Glacier	Total	User's Accuracy (%)
Dense Forest	50	0	0	0	0	60	100
Open Forest	0	50	0	0	0	50	100
Agriculture Fields	0	0	45	10	0	55	81.82
Wasteland	0	0	0	40	0	40	100
Snow/Glacier	0	0	5	0	50	55	90.91
Total	50	50	50	50	50	260	
Producer's Accuracy (%)	100	100	100	100	100		
						Overall Accuracy (%)	92.59

The user and producer accuracy assessment technique is adopted to assess the accuracy of classified map of the year 2000 and 2020. The accuracy assessment is performed using a high resolution global google earth engine satellite imagery by taken the random points with minimum 20 points in each class. The overall classification accuracy is found 95% and 92.59% for the classified image in the year of 2000 and 2020, respectively. The producer's and user's accuracy of various classified classes are presented in Table 4.2 and 4.3 for the year of 2000 and 2020, correspondingly. The 100% accuary is achived by the open forest and wasteland for the year 2000 and 2020. During the year 2000, the dense forest attained the classification accuracy is 83.33%, dense forest and snow/glacier is achieved 100 classification accuracy. However, the dense forest attained the classification accuracy is 100%, the agricultural fields and snow/glacier is attained the classification accuracy 81.82 % and 90.91 %, respectively of the year 2020. The change matrix generated for 2000 & 2020 also showed how much area of one class is converted into other class. There was increase in area open forest, and snow/glacier and and decrease in dense forest, agricultural land and wastelands. This shows that area increased at the open forested is reduction in dense forest due to the change in land surface temperature during the said time period. The increased in glacial area whereas the lower area of wasteland was covered up by grassland. The superiority of Evergreen forest reduced as huge area of dense forest became transformed to open forest.

CHAPTER 5

CONCLUSION

This study presented the Land use and Land cover changes along woth the changes in Land surface temperatures (LST) during the two decades (years 2000 to 2020) over the Garhwal region is the part of Uttarakhand Himalaya which occupies 32486 Km2 (60.67%) area and represented highly rugged and fragile topography. For this study, Landsat-8 OLI datasets are used for the gap ogf 10 year duration 2000 and 2020.

The following conclusions are drawn from the study,

1. The overall classification accuaracies are achived 95% and 92.59 during the classifications of the satellite imagery in various land covers like Dense forest, Open forest, Agricultural land, Wasteland and Swon/Glacier for the years of 2000 and 2020, respectively.
2. The increment in minimum and maximum mean Land surface temperature is found 2.04 K and 3.8 K for the proposed study area during 2000 to 2020.
3. The Dense forested area is degraded due to increment in the LST throughout the 2000 and 2020 years with 4.49 %.
4. The decrement in the dense forest area causes the increment open forest and snow cover area by the 0.39% and 4.787%, respectively.
5. The agricultural and waste land are also decreased with 0.184% and 0.503%, respectively.

REFERENCES

Anand, J., Sailor, D.J., and Baniassadi, A. (2021) The relative role of solar reflectance and thermal emittance for passive daytime radiative cooling technologies applied to rooftops. *Sustainable Cities and Society*, *65*, 102612.

Andersen, J., Dybkjaer, G., Jensen, K.H., Refsgaard, J., and Rasmussen, K. (2002) Use of remotely sensed precipitation and leaf area index in a distributed hydrological model. *Journal of Hydrology*, *264*, 34-50.

Ao, A., Changkija, S., and Tripathi, S. (2021) Stand structure, community composition and tree species diversity of sub-tropical forest of Nagaland, Northeast India. *Tropical Ecology*, 1-14.

Ball, M., and Pinkerton, H. (2006) Factors affecting the accuracy of thermal imaging cameras in volcanology. *Journal of Geophysical Research: Solid Earth*, 111.

Basso, B., Cammarano, D., and De Vita, P. (2004) Remotely sensed vegetation indices: Theory and applications for crop management. *Rivista Italiana di Agrometeorologia*, *1*, 36-53.

Breda, N.J. (2003) Ground-based measurements of leaf area index: a review of methods, instruments and current controversies. *Journal of Experimental Botany*, *54*, 2403-2417.

Carlson, T.N., and Ripley, D.A. (1997) On the relation between NDVI, fractional vegetation cover, and leaf area index. *Remote Sensing of Environment*, *62*, 241-252.

Chang, Y., Ding, Y., Zhao, Q., and Zhang, S. (2017) Remote estimation of terrestrial evapotranspiration by Landsat 5 TM and the SEBAL model in cold and high-altitude regions: a case study of the upper reach of the Shule River Basin, China. *Hydrological Processes*, *31*, 514-524.

Chen, J., Jönsson, P., Tamura, M., Gu, Z., Matsushita, B., and Eklundh, L. (2004) A simple method for reconstructing a high-quality NDVI time-series data set based on the Savitzky–Golay filter. *Remote Sensing of Environment*, *91*, 332-344.

Chen, J.M., and Black, T. (1992) Defining leaf area index for non-flat leaves. *Plant, Cell & Environment*, *15*, 421-429.

Chen, J.M., Rich, P.M., Gower, S.T., Norman, J.M., and Plummer, S. (1997) Leaf area index of boreal forests: Theory, techniques, and measurements. *Journal of Geophysical Research: Atmospheres*, *102*, 29429-29443.

D'Annunzio, R., Lindquist, E., and MacDicken, K.G. (2014) Global forest land-use change from 1990 to 2010: an update to a global remote sensing survey of forests. Food and Agriculture Organization of the United Nations. *Report from FAO and European Commission Joint Research Centre*, 6 p.

Davies, S.J., Abiem, I., Salim, K.A., Aguilar, S., Allen, D., Alonso, A., Anderson-Teixeira, K., Andrade, A., Arellano, G., and Ashton, P.S. (2021) ForestGEO: Understanding forest diversity and dynamics through a global observatory network. *Biological Conservation*, *253*, 108907.

de Almeida, C.L., de Carvalho, T.R.A., and de Araújo, J.C. (2019) Leaf area index of Caatinga biome and its relationship with hydrological and spectral variables. *Agricultural and Forest Meteorology*, *279*, 107705.

Dorji, T., Odeh, I.O., Field, D.J., and Baillie, I.C. (2014) Digital soil mapping of soil organic carbon stocks under different land use and land cover types in montane ecosystems, Eastern Himalayas. *Forest Ecology and Management*, *318*, 91-102.

Duffie, J.A., and Beckman, W.A. (1980) *Solar engineering of thermal processes*. Wiley New York.

Gamon, J.A., Field, C.B., Goulden, M.L., Griffin, K.L., Hartley, A.E., Joel, G., Penuelas, J., and Valentini, R. (1995) Relationships between NDVI, canopy structure, and photosynthesis in three Californian vegetation types. *Ecological Applications*, *5*, 28-41.

Garrard, R., Kohler, T., Price, M.F., Byers, A.C., Sherpa, A.R., and Maharjan, G.R. (2016) Land use and land cover change in Sagarmatha National Park, a world heritage site in the Himalayas of Eastern Nepal. *Mountain Research and Development*, *36*, 299-310.

Gilabert, M., González-Piqueras, J., Garcıa-Haro, F., and Meliá, J. (2002) A generalized soil-adjusted vegetation index. *Remote Sensing of Environment*, *82*, 303-310.

Grenfell, T.C., Warren, S.G., and Mullen, P.C. (1994) Reflection of solar radiation by the Antarctic snow surface at ultraviolet, visible, and near-infrared wavelengths. *Journal of Geophysical Research: Atmospheres*, *99*, 18669-18684.

Gyamfi-Ampadu, E., Gebreslasie, M., and Mendoza-Ponce, A. (2021) Evaluating Multi-Sensors Spectral and Spatial Resolutions for Tree Species Diversity Prediction. *Remote Sensing*, *13*, 1033.

He, K.S., Bradley, B.A., Cord, A.F., Rocchini, D., Tuanmu, M.N., Schmidtlein, S., Turner, W., Wegmann, M., and Pettorelli, N. (2015) Will remote sensing shape the next generation of species distribution models? *Remote Sensing in Ecology and Conservation*, *1*, 4-18.

Hu, X., Ren, H., Tansey, K., Zheng, Y., Ghent, D., Liu, X., and Yan, L. (2019) Agricultural drought monitoring using European Space Agency Sentinel 3A land surface temperature and normalized difference vegetation index imageries. *Agricultural and Forest Meteorology*, *279*, 107707.

Huete, A.R. (1988) A soil-adjusted vegetation index (SAVI). *Remote Sensing of Environment*, *25*, 295-309.

Irons, J.R., Dwyer, J.L., and Barsi, J.A. (2012) The next Landsat satellite: The Landsat data continuity mission. *Remote Sensing of Environment*, *122*, 11-21.

Ishtiaque, A., Shrestha, M., and Chhetri, N. (2017) Rapid urban growth in the Kathmandu Valley, Nepal: Monitoring land use land cover dynamics of a himalayan city with landsat imageries. *Environments*, *4*, 72.

Jaafar, H.H., and Ahmad, F.A. (2020) Time series trends of Landsat-based ET using automated calibration in METRIC and SEBAL: The Bekaa Valley, Lebanon. *Remote Sensing of Environment*, *238*, 111034.

Jenerette, G.D., Harlan, S.L., Buyantuev, A., Stefanov, W.L., Declet-Barreto, J., Ruddell, B.L., Myint, S.W., Kaplan, S., and Li, X. (2016) Micro-scale urban surface temperatures are related to land-cover features and residential heat related health impacts in Phoenix, AZ USA. *Landscape Ecology*, *31*, 745-760.

Jiang, Z., Huete, A.R., Li, J., and Qi, J. (2007) Interpretation of the modified soil-adjusted vegetation index isolines in red-NIR reflectance space. *Journal of Applied Remote Sensing*, *1*, 013503.

Kamran, K.V., Pirnazar, M., and Bansouleh, V.F., (2015) Land surface temperature retrieval from Landsat 8 TIRS: comparison between split window algorithm and SEBAL method, Third international conference on remote sensing and geoinformation of the environment (RSCy2015). *International Society for Optics and Photonics*, 953503 p..

Kergoat, L. (1998) A model for hydrological equilibrium of leaf area index on a global scale. *Journal of Hydrology*, *212*, 268-286.

Kimball, B. (2005) Theory and performance of an infrared heater for ecosystem warming. *Global Change Biology*, *11*, 2041-2056.

Le Moan, S., Mansouri, A., Voisin, Y., and Hardeberg, J.Y. (2011) A constrained band selection method based on information measures for spectral image color visualization. *IEEE Transactions on Geoscience and Remote Sensing, 49*, 5104-5115.

Li, S., and Zhao, W. (2010) Satellite-based actual evapotranspiration estimation in the middle reach of the Heihe River Basin using the SEBAL method. *Hydrological Processes, 24*, 3337-3344.

Lobovikov, M., Paudel, S., Ball, L., Piazza, M., Guardia, M., Ren, H., Russo, L., and Wu, J. (2007) World bamboo resources: a thematic study prepared in the framework of the global forest resources assessment 2005. *Food & Agriculture Org*.

Mackay, D., and Matsugu, R.S. (1973) Evaporation rates of liquid hydrocarbon spills on land and water. *The Canadian Journal of Chemical Engineering, 51*, 434-439.

Mackey, B., Kormos, C.F., Keith, H., Moomaw, W.R., Houghton, R.A., Mittermeier, R.A., Hole, D., and Hugh, S. (2020) Understanding the importance of primary tropical forest protection as a mitigation strategy. *Mitigation and Adaptation Strategies for Global Change, 25*, 763-787.

Mayaux, P., Achard, F., and Malingreau, J.P. (1998) Global tropical forest area measurements derived from coarse resolution satellite imagery: a comparison with other approaches. *Environmental Conservation, 25*, 37-52.

Mildrexler, D.J., Zhao, M., and Running, S.W. (2011) A global comparison between station air temperatures and MODIS land surface temperatures reveals the cooling role of forests. *Journal of Geophysical Research: Biogeosciences, 116*.

Mishra, P.K., Rai, A., and Rai, S.C. (2020) Land use and land cover change detection using geospatial techniques in the Sikkim Himalaya, India. *The Egyptian Journal of Remote Sensing and Space Science*, *23*, 133-143.

Morgan, B.E., Chipman, J.W., Bolger, D.T., and Dietrich, J.T. (2021) Spatiotemporal Analysis of Vegetation Cover Change in a Large Ephemeral River: Multi-Sensor Fusion of Unmanned Aerial Vehicle (UAV) and Landsat Imagery. *Remote Sensing*, *13*, 51.

Munsi, M., Areendran, G., Ghosh, A., and Joshi, P. (2010) Landscape characterisation of the forests of Himalayan foothills. *Journal of the Indian Society of Remote Sensing*, *38*, 441-452.

Myneni, R.B., Ramakrishna, R., Nemani, R., and Running, S.W. (1997) Estimation of global leaf area index and absorbed PAR using radiative transfer models. *IEEE Transactions on Geoscience and Remote Sensing*, *35*, 1380-1393.

Nemani, R., Pierce, L., Running, S., and Band, L. (1993) Forest ecosystem processes at the watershed scale: sensitivity to remotely-sensed leaf area index estimates. *International Journal of Remote Sensing*, *14*, 2519-2534.

Newbold, T., Hudson, L.N., Phillips, H.R., Hill, S.L., Contu, S., Lysenko, I., Blandon, A., Butchart, S.H., Booth, H.L., and Day, J. (2014) A global model of the response of tropical and sub-tropical forest biodiversity to anthropogenic pressures. *Proceedings of the Royal Society B: Biological Sciences*, *281*, 20141371.

Patel, N., Parida, B., Venus, V., Saha, S., and Dadhwal, V. (2012) Analysis of agricultural drought using vegetation temperature condition index (VTCI) from Terra/MODIS satellite data. *Environmental Monitoring and Assessment*, *184*, 7153-7163.

Pettorelli, N., Laurance, W.F., O'Brien, T.G., Wegmann, M., Nagendra, H., and Turner, W. (2014) Satellite remote sensing for applied ecologists: opportunities and challenges. *Journal of Applied Ecology*, *51*, 839-848.

Pettorelli, N., Vik, J.O., Mysterud, A., Gaillard, J.-M., Tucker, C.J., and Stenseth, N.C. (2005) Using the satellite-derived NDVI to assess ecological responses to environmental change. *Trends in Ecology & Evolution*, *20*, 503-510.

Putz, F.E., and Redford, K.H. (2010) The importance of defining 'forest': Tropical forest degradation, deforestation, long-term phase shifts, and further transitions. *Biotropica*, *42*, 10-20.

Rasool, R., Fayaz, A., ul Shafiq, M., Singh, H., and Ahmed, P. (2021) Land use land cover change in Kashmir Himalaya: Linking remote sensing with an indicator based DPSIR approach. *Ecological Indicators*, *125*, 107447.

Recio, J., Hermosilla, T., and Ruiz, L. (2012) Automated extraction of agronomic parameters in orchard plots from high-resolution imagery. *Options Méditerranéennes, Série B. Etudes et Recherches*, *67*,161-174.

Ren, H., Zhou, G., and Zhang, F. (2018) Using negative soil adjustment factor in soil-adjusted vegetation index (SAVI) for aboveground living biomass estimation in arid grasslands. *Remote Sensing of Environment*, *209*, 439-445.

Rondeaux, G., Steven, M., and Baret, F. (1996) Optimization of soil-adjusted vegetation indices. *Remote Sensing of Environment*, *55*, 95-107.

Roy, L., and Das, S. (2021) GIS-based landform and LULC classifications in the Sub-Himalayan Kaljani Basin: Special reference to 2016 Flood. *The Egyptian Journal of Remote Sensing and Space Science*.

Ryu, Y., Sonnentag, O., Nilson, T., Vargas, R., Kobayashi, H., Wenk, R., and Baldocchi, D.D. (2010) How to quantify tree leaf area index in an open

savanna ecosystem: a multi-instrument and multi-model approach. *Agricultural and Forest Meteorology, 150*, 63-76.

Setiawan, H.R., and Masitah, W. (2017) Meningkatkan Motivasi dan Hasil Belajar Mahasiswa Melalui Model Pembelajaran Kooperatif Group Investigation Pada Mata Kuliah Psikologi Pendidikan di Program Studi Pendidikan Agama Islam FAI UMSU 2016-2017. *Intiqad: Jurnal Agama dan Pendidikan Islam, 9*, 47-67.

Sobrino, J.A., Jiménez-Muñoz, J.C., Sòria, G., Romaguera, M., Guanter, L., Moreno, J., Plaza, A., and Martínez, P. (2008) Land surface emissivity retrieval from different VNIR and TIR sensors. *IEEE Transactions on Geoscience and Remote Sensing, 46*, 316-327.

Taubert, F., Fischer, R., Groeneveld, J., Lehmann, S., Müller, M.S., Rödig, E., Wiegand, T., and Huth, A. (2018) Global patterns of tropical forest fragmentation. *Nature, 554*, 519-522.

Tucker, C.J., Pinzon, J.E., Brown, M.E., Slayback, D.A., Pak, E.W., Mahoney, R., Vermote, E.F., and El Saleous, N. (2005) An extended AVHRR 8-km NDVI dataset compatible with MODIS and SPOT vegetation NDVI data. *International Journal of Remote Sensing, 26*, 4485-4498.

Ullah, S., Ahmad, K., Sajjad, R.U., Abbasi, A.M., Nazeer, A., and Tahir, A.A. (2019) Analysis and simulation of land cover changes and their impacts on land surface temperature in a lower Himalayan region. *Journal of Environmental Management, 245*, 348-357.

Van de Griend, A., and Owe, M. (1993) On the relationship between thermal emissivity and the normalized difference vegetation index for natural surfaces. *International Journal of Remote Sensing, 14*, 1119-1131.

Venancio, L.P., Mantovani, E.C., do Amaral, C.H., Neale, C.M.U., Gonçalves, I.Z., Filgueiras, R., and Campos, I. (2019) Forecasting corn yield at the farm level

in Brazil based on the FAO-66 approach and soil-adjusted vegetation index (SAVI). *Agricultural Water Management*, *225*, 105779.

Wan, Z., Wang, P., and Li, X. (2004) Using MODIS land surface temperature and normalized difference vegetation index products for monitoring drought in the southern Great Plains, USA. *International Journal of Remote Sensing*, *25*, 61-72.

Warren, S.G. (1982) Optical properties of snow. *Reviews of Geophysics*, *20*, 67-89.

Waters, R., Allen, R., Bastiaanssen, W., Tasumi, M., and Trezza, R. (2002) Sebal. Surface Energy Balance Algorithms for Land. Idaho Implementation. *Advanced Training and Users Manual*, Idaho, USA.

Zaitunah, A., and Sahara, F. (2021) Mapping and assessment of vegetation cover change and species variation in Medan, North Sumatra. *Heliyon*, *7*, e07637.

Zhu, Z., and Woodcock, C.E. (2014) Continuous change detection and classification of land cover using all available Landsat data. *Remote Sensing of Environment*, *144*, 152-171.